# Cinnamaldehyde and cuminaldehyde thiosemicarbazones and their copper(II) and nickel(II) complexes: A study to understand their biological activity

**ARTICLE** *in* JOURNAL OF INORGANIC BIOCHEMISTRY · NOVEMBER 2014

Impact Factor: 3.44 · DOI: 10.1016/j.jinorgbio.2014.07.014



**9 AUTHORS**, INCLUDING:

Franco Bisceglie
Università degli studi di Parma
**41** PUBLICATIONS **1,129** CITATIONS
SEE PROFILE

Silvana Pinelli
Università degli studi di Parma
**70** PUBLICATIONS **1,522** CITATIONS
SEE PROFILE

Antonio Mutti
Università degli studi di Parma
**358** PUBLICATIONS **6,653** CITATIONS
SEE PROFILE

Giorgio Pelosi
Università degli studi di Parma
**138** PUBLICATIONS **2,552** CITATIONS
SEE PROFILE

Journal of Inorganic Biochemistry 140 (2014) 111–125

Contents lists available at ScienceDirect

Journal of Inorganic Biochemistry

journal homepage: www.elsevier.com/locate/jinorgbio

# Cinnamaldehyde and cuminaldehyde thiosemicarbazones and their copper(II) and nickel(II) complexes: A study to understand their biological activity

Franco Bisceglie [a,b], Silvana Pinelli [b,c], Rossella Alinovi [b,c], Matteo Goldoni [c,d], Antonio Mutti [c], Alessandro Camerini [a], Lorenzo Piola [a], Pieralberto Tarasconi [a,b], Giorgio Pelosi [a,b,*]

[a] Department of Chemistry, University of Parma, Parco Area delle Scienze 17/A, 43124 Parma, Italy
[b] C.I.R.C.M.S.B. — Consorzio Interuniversitario di Ricerca in Chimica dei Metalli nei Sistemi Biologici, Parma Local Unit, 43124 Parma, Italy
[c] Department of Clinical and Experimental Medicine, University of Parma, Via Gramsci 14, 43126 Parma, Italy
[d] Workers Compensation Authority (INAIL), Research Center at the University of Parma, Via Gramsci 14, 43126 Parma, Italy

ARTICLE INFO

*Article history:*
Received 9 April 2014
Received in revised form 15 July 2014
Accepted 15 July 2014
Available online 23 July 2014

*Keywords:*
Thiosemicarbazone
Nickel
Copper
Caspase
DNA
Topoisomerase IIa

ABSTRACT

This paper reports the synthesis and characterization of *trans*-cinnamaldehyde thiosemicarbazone (Htcin), cuminaldehyde thiosemicarbazone (Htcum) and their copper and nickel complexes. All the compounds, which on healthy cells (human fibroblasts) show a neglectable cytotoxicity, were screened in vitro in cell line U937 for their antileukemic activity. These compounds, in spite of their molecular similarity, present variegated behaviors. Htcin shows no inhibition activity in U935 cells, while both its metal complexes inhibit proliferation with $IC_{50}$ at μM concentrations. The other ligand, Htcum, and its metal complexes, besides inhibiting proliferation, induce apoptosis. The cell cycle analysis highlights a $G_2$/M checkpoint stop suggesting a possible direct action on DNA or on topoisomerase IIa. From CD and UV spectroscopy experiments, the DNA results to be not the main target of all these molecules, while both copper complexes are effective topoisomerase IIa inhibitors. All of these molecules activate caspase-9 and caspase-3, while caspase-8 activity is significantly induced by both cinnamaldehyde metal complexes. Tests on PgP and intracellular metal concentrations (determined by mean of atomic absorption spectrometry) show that the compounds tend to accumulate in the cytoplasm and that the cells do not manage to pump out copper and nickel ions.



## 1. Introduction

Natural products have been a continuing source of novel drug leads [1] and, in this context, cinnamaldehyde has been tested for its anticancer activity [2]. This molecule has recently shown very interesting results in cell cultures and animal models, but only at high doses not achievable through simple dietary intake [3]. Also cuminaldehyde has been under study to verify its effectiveness as an antitumor agent and has shown good results on cultured murine but not on cultured human cells [4].

On this basis, and with the aim to overcome the limits owned by the free aldehydes, we decided to modify their structure endowing them with donor atoms in order to render them potential ligands for metal ions.

The derivatives we synthesized belong to the thiosemicarbazone family, which represents an interesting class of compounds (many of them being patented [5]) with a wide range of pharmacological applications thanks to their antibacterial, antiviral and antitumor activities [6–9]. In many cases, upon coordination to metal ions, the bioactivity of these compounds increases suggesting that complexation can be an interesting strategy of dose reduction [10–13]. Recently our studies addressed the synthesis of new SN chelating thiosemicarbazones derived from natural aldehydes such as citronellal, citral, octenal, retinal and their copper and nickel complexes [10,11,14–17]. We have then aimed our attention at the synthesis of new nickel and copper complexes of thiosemicarbazones derived from natural *trans*-cinnamaldehyde and cuminaldehyde (Htcin and Htcum). The corresponding thiosemicarbazones have also revealed antimicrobial and, more specifically, anti-tyrosinase activities [18,19] and many studies have been performed on DNA binding and nuclease activity of Cu(I) and Cu(II), and Pd(II) and Pt(II) complexes [20–22]. In the present work, after having synthesized and characterized cinnamaldehyde and cuminaldehyde thiosemicarbazones (Htcin **1** and Htcum **2**) together with their Ni(II) and Cu(II) complexes ([$Ni(tcin)_2$] **3**, [$Ni(tcum)_2$] **4**, [Cu(tcin)$Cl(OH_2)$] **5** and [Cu(tcum)$Cl(OH_2)$] **6**), a series of biological assays were performed. We started from a comparison between their proliferation inhibition on human histiocytic lymphoma cell line U937 vs human fibroblasts (non-cancer cells) and, subsequently, we carried out a series of more specific tests such as metal accumulation in the cytoplasm, Pgp protein activation, cell cycle assay, caspase-3, -8, and -9 assays, reactive oxygen species (ROS) determination, DNA interaction and topoisomerase IIa inhibition.

* Corresponding author. Fax: +39 0521905420.
*E-mail address:* giorgio.pelosi@unipr.it (G. Pelosi).

http://dx.doi.org/10.1016/j.jinorgbio.2014.07.014
0162-0134/

## 2. Experimental

### 2.1. Syntheses and characterizations

*trans*-Cinnamaldehyde (3-phenyl-2-propenal), cuminaldehyde (p-isopropyl benzaldehyde), thiosemicarbazide, nickel(II) acetate tetrahydrate and copper(II) chloride were purchased from Aldrich. C, H, N, and S analyses were obtained with a Carlo-Erba 1108 instrument. IR spectra were recorded using KBr pellets on a Nicolet 5PC FT-IR spectrophotometer, or using the compounds directly on the STR (attenuated total reflectance) accessory in the 4000–400 $cm^{-1}$ range. The relative intensity of reported FT-IR signals is defined as s = strong, br = broad, m = medium, and w = weak. $^1H$ NMR spectra were recorded on a Bruker Avance spectrometer at 300 MHz with TMS (tetramethylsilane) as the internal reference. The splitting of proton resonances in the reported $^1H$ NMR spectra is defined as s = singlet, br s = broad singlet, d = doublet, t = triplet, and m = multiplet. Melting points were determined with a Gallenkamp instrument (Weiss-Gallenkamp). Circular dichroism (CD) spectra were recorded at 25 °C on a Jasco J-715 spectropolarimeter. UV measurements were performed on a Varian UV–visible (UV–vis) Cary 50 spectrometer with quartz cuvettes.

#### 2.1.1. Preparation of the ligands

The ligands were prepared following a modified simple procedure [18,22–24]. Briefly: to 20 mL of a hot stirred ethanol solution of thiosemicarbazide (0.21 g, 2.3 mmol) an amount of 0.29 mL (2.3 mmol) of *trans*-cinnamaldehyde (3-phenyl-2-propenal), or 0.39 mL (2.3 mmol) of cuminaldehyde (p-isopropyl benzaldehyde) was added. In this way *trans*-cinnamaldehyde thiosemicarbazone (Htcin·$H_2O$, **1**) and cuminaldehyde thiosemicarbazone (Htcum, **2**) reported in Scheme 1 were synthesized. The mixture was refluxed for 7–9 h and then cooled to room temperature by slow evaporation. Both compounds were isolated as yellow crystals suitable for X-ray crystallography.

*2.1.1.1. trans-Cinnamaldehyde thiosemicarbazone Htcin·$H_2O$ (**1**).* Yield: 91%. Mp: 139 °C. FT-IR (KBr, $cm^{-1}$) 3416, s, 3260, m, 3154, m, $\nu$(NH); 3042, mw, $\nu$(CHaromatic); 1630, ms, $\nu$(C═N); 1621, ms, $\nu$(C═C); 820, w, $\nu$(CS). Anal. calc. for $C_{10}H_{13}N_3OS$: C 53.78; H 5.87; N 18.81; S 14.36. Found: C 53.65; H 5.35; N 19.12; S 14.53%. $^1H$ NMR data (δ, ppm; DMSO d6): 6.68 (m, 1 H, CH═C); 7.06 (d, 1 H, CH═C); 7.30–7.60 (m, 6 H, aromatic o and m, and $NH_2$); 7.90 (d, 1H, aromatic p); 8.17 (m, 1 H, CH═N); 11.38 (br, 1H, NH–C═S). $^{13}C$ NMR data (δ, ppm; DMSO d6): 178 (C═S); 145 (C═N); 139 (*C*═C–C); 136 (aromatic *C*–C═C); 129 and 127 (ortho and meta aromatic *C*); 125 (═*C*–C═N). UV–visible (solvent MeOH): 297 nm (n → π*), 246 nm (n → σ*); (solvent DMSO): 324 nm (π → π*), 241 nm (n → σ*).

*2.1.1.2. Cuminaldehyde thiosemicarbazone Htcum (**2**).* Yield: 86%. Mp: 144 °C. FT-IR (KBr, $cm^{-1}$) 3411, m, 3280, m, $\nu$(NH); 3013, m, $\nu$(CHaromatic); 2957, mw, $\nu$(CHaliphatic), 1586, s, $\nu$(C═N); 820, s, $\nu$(CS). Anal. calc. for $C_{11}H_{15}N_3S$: C 59.64; H 6.78; N 18.98; S 14.48. Found: C 59.54; H 6.62; N 18.67; S 14.19%. $^1H$ NMR data (δ, ppm; DMSO d6): 1.23 (d, 6 H, CH3); 2.89 (ept, 1H, CH isopropyl); 7.27, 7.30 (2s, 2H, aromatic); 7.70 (m, 2H, aromatic); 7.93 and 8.03 (2s, 2H, $NH_2$); 8.17 (s, 1H, CH═N); 11.34 (br, 1H, NH–C═S). $^{13}C$ NMR data (δ, ppm; DMSO d6): 178 (C═S); 150 (para aromatic C); 143 (C═N); 132 (aromatic *C*–C═N); 127 (ortho and meta aromatic *C*); 33 (*C*H($CH_3$)$_2$); 24 (2 $CH_3$). UV–visible (solvent MeOH): 312 nm (n → π*), 223 nm (n → σ*); (solvent DMSO): 311 nm (n → π*), 240 nm (n → σ*).

#### 2.1.2. Preparation of the complexes

A schematic pictogram of complex syntheses is reported in Scheme 2. To 20 mL of a hot stirred ethanol solution of the proper ligand an amount of nickel(II) acetate tetrahydrate in a 1:2 molar ratio of Ni: ligand was added (0.500 g of the ligand, 2.24 mmol, and 0.28 g of metal salt, 1.12 mmol) for **3** (0.610 g of the ligand, 2.76 mmol, and 0.343 g of metal salt, 1.38 mmol), for **4** together with additional 20 mL of ethanol. The mixture was allowed to reach the reflux temperature. When the inorganic salt was completely dissolved, the resulting solution changed the color from pale yellow to brown and was left under magnetic stirring for 1 h. The solution was then cooled down to room temperature. Powdered solids obtained by cooling were filtered and characterized by elemental analysis as Ni(tcin)$_2$·$H_2O$. A slow evaporation of the mother liquor solution afforded needle-shaped crystals suitable for X-ray diffraction studies that were identified later as [Ni(tcin)$_2$]·$2C_2H_5OH$. Copper(II) complexes were synthesized dissolving the proper ligand (0.237 g, 1.16 mmol for Htcin **1** and 0.263 g, 1.18 mmol for Htcum **2**) in 50 mL of boiling ethanol and adding the equimolar amount of $CuCl_2$·$2H_2O$ (0.197 g, 1.16 mmol to ligand **1** and 0.203 g, 1.19 mmol to ligand **2**) dissolved in 20 mL of ethanol. The resulting green solutions were refluxed for 1 h and then left to cool to room temperature under magnetic stirring for 8 h. The green powder formed during cooling was then filtered and dried under vacuum.

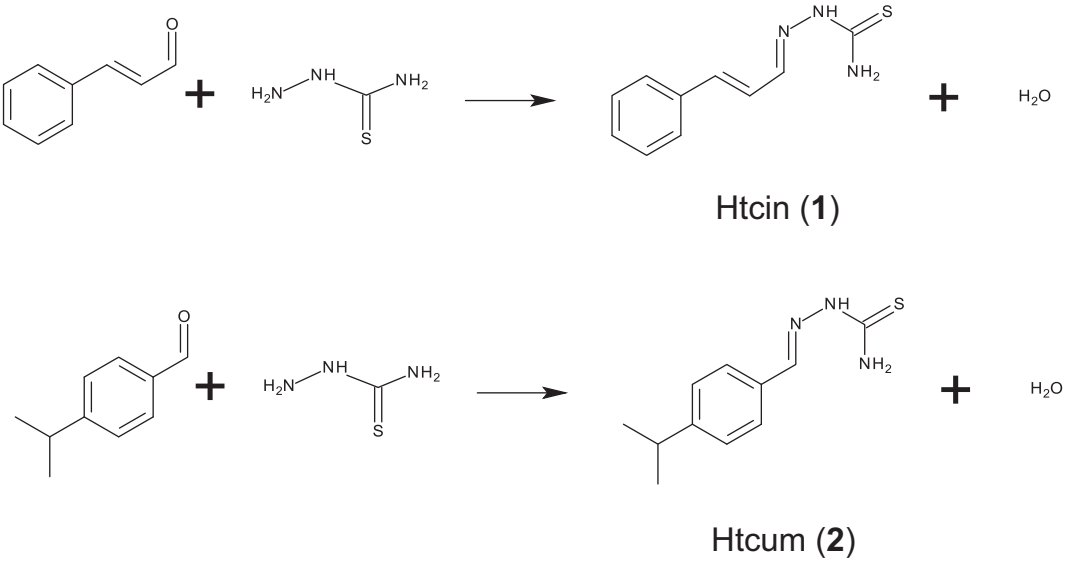


**Scheme 1.** Syntheses of compounds **1** and **2**

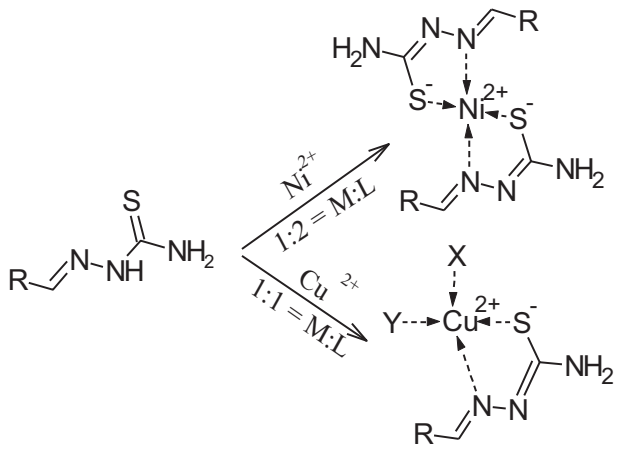


**Scheme 2.** Schematic view of the syntheses of [Ni(tcin)$_2$] **3**, [Ni(tcum)$_2$] **4**, [Cu(tcin)XY] **5** and [Cu(tcum)XY] **6**. X and Y = $Cl^-$ and $H_2O$ respectively. R is (2E)-3-phenylprop-2-en-1-yl for (tcin) derivatives and 4-isopropylphenyl for (tcum) ones.

*2.1.2.1. [Ni(tcin)$_2$]·$H_2O$ (**3**).* Yield: 74%. Mp: 146 °C. FT-IR (KBr, $cm^{-1}$) 3384, w, 3280, m, and 3153, w, ν(NH); 1620, s, ν(C═N); 778, m, ν(CS). Anal. calc. for $C_{20}H_{22}N_6OS_2Ni$: C 49.50; H 4.57; N 17.32; S 13.22. Found: C 49.72; H 4.61; N 17.00; S 13.23%. $^1$H NMR data (δ, ppm; DMSO-d6): 6.95 (s, 2 H, CH═C); 7.20 (bs, 2H, $NH_2$); 7.53 (m, 1 H, CH═N); 7.51–7.38 (m, 5 H, aromatic). $^{13}$C NMR data (δ, ppm; DMSO d6): 142 (C═N); 130 (*C*═C–C); 136 (aromatic *C*–C═C); 129 and 128 (ortho and meta aromatic *C*); 120 (═*C*–C═N). UV–visible (solvent DMSO):488 nm (d → d), 367 nm (n → π*), 327 nm (π → π*), 254 nm (n → σ*).

*2.1.2.2. [Ni(tcum)$_2$] (**4**).* Yield: 62%. Mp: 176 °C. FT-IR (KBr, $cm^{-1}$) 3435, w, 3279, w, 3157, w, ν(NH); 3045, mw, 3027, mw, ν(CHaromatic); 2967, mw, 2956, m, ν(CH); 1603, m, ν(C(═S)–N); 1577, m, ν(C═N); 795, s, ν(CS). Anal. calc. for $C_{22}H_{28}N_6S_2Ni$: C 52.92; H 5.65; N 16.83; S 12.84. Found: C 52.65; H 5.50; N 17.11; S 12.95%. $^1$H NMR data (δ, ppm; DMSO-d6): 1.20 (d, 6 H, CH3); 2.89 (ept, 1H, CH isopropyl); 7.09 (1bs, 2H, $NH_2$); 7.29 (m, 3H, 2 H aromatic, m, +CH═N); 8.10 (d, 2H, aromatic, o). $^{13}$C NMR data (δ, ppm; DMSO d6): 152 (para aromatic C); 133 (C═N); 131 (aromatic *C*–C═N); 127 (o and m aromatic *C*); 34 (*C*H($CH_3$)$_2$); 24 (2 $CH_3$). UV–visible (solvent DMSO): 450 nm (d → d), 375 nm (n → π*), 321 nm (π → π*), 254 nm (n → σ*).

*2.1.2.3. [Cu(tcin)($H_2O$)Cl] (**5**).* Yield: 57%. Mp: 150 °C. FT-IR (KBr, $cm^{-1}$) 3375, w, 3262, m, and 3164, w br, ν(NH); 1608, s, ν(C═N); 808, m, ν(CS). Anal. calc. for $C_{10}H_{12}N_3OSCuCl$: C 37.38; H 3.76; N 13.08; S 9.98. Found: C 37.56; H 4.01; N 12.79; S 10.15%. UV–visible (solvent DMSO):366 nm (n → π*), 265 nm (π → π*).

*2.1.2.4. [Cu(tcum)($H_2O$) Cl] (**6**).* Yield: 69%. Mp: 156 °C. FT-IR (KBr, $cm^{-1}$) 3427, m, 3265, w br, 3137, w, ν(NH); 3013, m, ν(CHaromatic); 2957, mw, ν(CHaliphatic), 1602, m, ν(C(═S)–N); 1560, m, ν(C═N); 829, s, ν(CS). Anal. calc. for $C_{11}H_{16}N_3SCuCl$: C 39.17; H 4.78; N 12.46; S 9.50. Found: C 39.47; H 5.02; N 12.56; S 9.93%. UV–visible (solvent DMSO):380 nm (n → π*), 314 nm (π → π*), 240 nm (n → σ*).

### 2.1.3. Crystallographic data

Relevant data concerning collection and details of structure refinement are reported in the SI. Intensity data for all compounds were collected on a SMART 1000 Bruker AXS diffractometer with Mo-Kα radiation and absorption corrections were carried out using the SADABS [25] procedure. For ligand **1** data were collected at low temperature (123 K). The structures were solved using direct methods (SIR-97 [26]). Refinements were carried out by full matrix least-squares cycles SHELXL97 [27] for all compounds. Crystal data are reported in Table 1. All calculations were performed using WinGX [28]. The program PARST [29] was employed for the geometrical description and PLUTON [30] and MERCURY [31] for the drawings. CCDC 939343–939346 contain the supplementary crystallographic data for compounds **1**, **2**, **3** and **4**. These data can be obtained free of charge via http://www.ccdc.cam.ac.uk/conts/retrieving.html, or from the Cambridge Crystallographic Data Centre, 12 Union Road, Cambridge CB2 1EZ, UK; fax: (+44) 1223-336-033, or e-mail: deposit@ccdc.cam.ac.uk.

### 2.1.4. DNA binding studies: UV–vis and CD titrations

Circular dichroism (CD) spectra were recorded at 25 °C on a Jasco J-715 spectropolarimeter with buffer compensation; each spectrum is the average of three independent measurements. 1 cm path-length

**Table 1**
Crystal data for compounds **1**, **2**, **3** and **4**.

| Compound | (**1**) | (**2**) | (**3**) | (**4**) |
|---|---|---|---|---|
| Formula | $C_{10}H_{13}N_3O_1S_1$ | $C_{11}H_{15}N_3S_1$ | $C_{24}H_{32}N_6NiO_2S_2$ | $C_{22}H_{28}N_6NiS_2$ |
| Molecular mass | 223.292 | 221.320 | 559.386 | 499.334 |
| Space group | $P2_12_12_1$ | $P2_1/c$ | $P$-1 | $P2_1/a$ |
| *a* (Å) | 6.209(1) | 14.463(3) | 6.607(2) | 7.194(1) |
| *b* (Å) | 7.754(1) | 5.643(1) | 10.882(4) | 11.389(2) |
| *c* (Å) | 24.555(2) | 14.481(3) | 10.906(4) | 14.873(2) |
| α (°) | 90 | 90 | 114.37(1) | 90 |
| β (°) | 90 | 94.761(3) | 90.54(1) | 101.018(2)(1) |
| γ (°) | 90 | 90 | 97.15(1) | 90 |
| V (Å$^3$) | 1182.1(2) | 1177.8(4) | 707.1(4) | 1196.1(3) |
| *Z* | 4 | 4 | 1 | 2 |
| F(000) | 472 | 472 | 294 | 524 |
| $D_{calc}$ (Mg/m$^3$) | 1.255 | 1.248 | 1.314 | 1.38 |
| μ (mm$^{-1}$) | 0.252 | 0.247 | 0.864 | 1.007 |
| λ (Å) | 0.71069 | 0.71069 | 0.71069 | 0.71069 |
| Radiation | Mo Kα | Mo Kα | Mo Kα | Mo Kα |
| *θ* range (°) | 1.7–23.3 | 2.8–27.0 | 2.1–23.5 | 1.39–31.92 |
| hkl range | −6, 6; −8, 8; −27, 27 | −17, 18; −7, 7; −18, 18 | −7, 7; −12, 12; −12, 12 | −10, 10; −16, 16; −21, 21 |
| Cryst. size (mm) | 0.4 0.4 0.3 | 0.5 0.5 0.5 | 0.5 0.2 0.2 | 0.4 0.2 0.1 |
| No. of meas. refl. | 9730 | 8974 | 5831 | 3947 |
| No. of unique refl. | 1692 | 2550 | 2080 | 2304 |
| No. of refined param. | 188 | 196 | 179 | 198 |
| Max. & min res. (eÅ$^{-3}$) | 0.12, −0.12 | 0.28, −0.44 | 0.66, −0.81 | 0.42, −0.28 |
| $R = \Sigma\|\|F_o\| - \|F_c\|\|/\Sigma\|F_o\|$ | 0.040 | 0.049 | 0.0527 | 0.0490 |
| Rw2 | 0.075 | 0.144 | 0.1304 | 0.1016 |

quartz cuvettes were used. UV–vis studies were performed on a Varian Cary50. Disodium salt of calf-thymus (CT) DNA (Serva) was used as received and stored at 4 °C. Solutions of DNA in 10 mM of phosphate buffered saline (PBS) (pH = 7.4) 137 mM NaCl, 2.7 mM KCl gave a ratio of UV absorbance at 260 and 280 nm, A260/A280, of 1.9, indicating that the DNA was sufficiently free of protein. Concentrated stock solutions of DNA [NP] were determined by UV absorbance at 260 nm. The extinction coefficient, $\varepsilon_{260}$, was taken as 6600 $M^{-1}$ $cm^{-1}$ [32]. Stock solutions were stored at 4 °C and used after no more than 4 days. All the compounds were dissolved in DMSO. The final concentration of DMSO in the buffered solution never exceeds 5%.

### 2.2. Biological assays

#### 2.2.1. Cell growth

The U937 cells, a human histiocytic lymphoma cell line, obtained from the American Type Culture Collection (ATCC, Rockville, MD, USA) were maintained in RPMI-1640 medium (Gibco-BRL, Life Technologies, Carlsbad, CA, USA) supplemented with 10% (v/v) fetal bovine serum, 100 units/mL penicillin, 100 μg/mL streptomycin, and 2 mM L-glutamine at 37 °C in a humidified atmosphere containing 5% $CO_2$. Human foreskin fibroblasts (kindly provided by Prof. O. Bussolati, University of Parma) were grown in DMEM, supplemented with 10% FBS.

#### 2.2.2. Cytotoxicity assays

The effects of compounds on cell viability were evaluated using MTS (3-(4,5-dimethylthiazol-2-yl)-5-(3-carboxymethoxyphenyl)-2-(4-sulfophenyl)-2H-tetrazolium, inner salt), in the form of the CellTiter 96® AQueous Cell Proliferation Assay kit (Promega, Madison, WI, USA). The assay was performed according to the manufacturer's instructions. Briefly, U937 cells in exponential phase were seeded at a density of $1.5 \times 10^4$ cells/100 μL in 96 well plates and incubated for 24 h before the treatment with increasing concentrations of ligands or complexes, reconstituted in DMSO and diluted in RPMI 1640 medium (working range 0.1–100 μM). The cells were then incubated for 24 h in the test drug and proliferation/viability assessed by the addition of MTS reagent. The absorbance was read after 1 h at 490 nm by a Multiskan Ascent photometer (Thermo Labsystems, Helsinki, Finland). At least three independent experiments were performed with eight replicate wells per sample and the results were presented as mean ± SD. The net absorbance from the wells of untreated cells was taken as the 100% viability value. The morphology of cells was monitored under an inverted microscope (Olympus CK40-RFL, Tokyo, Japan) at 6, 12, 24 and 48 h. Cell viability was also monitored by counting viable cells in a hemocytometer (Trypan blue exclusion); after 24 h incubation with compounds, the cells collected from eight wells were pooled and placed in Trypan blue for 5 min.

#### 2.2.3. Apoptosis

For apoptosis assays, U937 cells were seeded at $1.5 \times 10^5$ cells/mL. After 24 h the cells in the exponential phase of growth were treated with ligands and complexes at $IC_{50}$ concentrations for different periods (6–48 h).

#### 2.2.4. Flow cytometric analysis of apoptosis

The Annexin V/FITC kit assay (Bender MedSystems GmbH, Vienna, Austria) was used. After 6, 12, 24 and 48 h of treatment $1 \times 10^5$ cells were washed in PBS, incubated with FITC-labeled Annexin V and propidium iodide (PI) at room temperature for 15 min in the dark and analyzed using a flow cytometer (FACSCalibur, BD, Franklin Lakes, NJ, USA).

#### 2.2.5. Assay of caspase-3, -8 and -9 activities

The enzymatic activity of the caspases was assayed in 96 well-microtiter plates using Fluorometric Assay Kits, produced by Biovision (Biovision, Mountain View, CA, USA) for caspase-8 and caspase-9 and by Molecular Probes (Molecular Probes, Eugene, OR, USA) for caspase-3. A sample of $3 \times 10^6$ of treated cells were pelleted by centrifugation and resuspended in lysis buffer in an ice bath. The lysates were incubated in the reaction buffer with the corresponding substrates: Ile-Glu-Thr-Asp (IETD)-AFC (7-amino-4-trifluoromethyl coumarin) for caspase-8, Leu-Glu-His-Asp (LEHD)-AFC for caspase-9 and rhodamine 110 bis-(N-CBZ-L-aspartyl-L-glutamyl-L-valyl-L-aspartic acid amide) (Z-DEVD-R110) for caspase-3, according to the manufacturers' protocols. Upon enzymatic cleavage the substrates were converted into fluorescent products, which were quantified by a Cary Eclipse fluorescence spectrophotometer (Varian, Inc., Palo Alto, CA, USA). In caspase-3 assay a R110 standard curve (range 0–25 μM) was prepared. Results of caspase-8 and -9 were expressed in arbitrary units. All data were expressed relative to the protein content. Fold-increase in caspase activity was determined by comparing the results with the level of the uninduced control.

#### 2.2.6. DNA fragmentation assay

After a 24 h treatment, $1 \times 10^6$ cells were washed twice with PBS and centrifuged. The pellets were resuspended in 20 μL of lysis buffer solution (50 mM Tris–HCl pH 8.0, 10 mM EDTA and 0.5% sodium laurylsarkosinate) and then incubated with Proteinase K (4 mg/mL) and RNAse (2 mg/mL) at different temperatures. Ten μl of loading buffer (10 mM EDTA pH 8, 1% agarose, 0.25% bromophenol blue, 40% sucrose) was subsequently added to each sample. The fragments of extracted DNA were separated by electrophoresis on a 2% agarose gel containing ethidium bromide 0.1 μg/mL. The gels were observed and photographed under ultraviolet light by a Fluor-S™ MultiImager (Bio-Rad, Hercules; CA, USA).

#### 2.2.7. Determination of ROS

The level of intracellular ROS was measured by the change in fluorescence resulting from oxidation of 2,7-dichlorofluorescein diacetate (DCFH-DA) (Molecular Probes, Eugene, OR, USA), a non-polar and non-fluorescent compound that can diffuse through the cell membrane [33]. After the dye had entered the cells, the acetate group on DCFH-DA is cleaved by intracellular esterases, to yield polar, non-fluorescent 2′,7′-dichlorofluorescein (DCFH). DCFH is trapped within the cytoplasm, where it can react with ROS to form the highly fluorescent two-electron oxidation product 2′,7′-dichlorofluorescein (DCFH). To load cells with DCFH-DA, culture medium was replaced with pre-warmed PBS containing 10 μm DCFH-DA and incubated at 37 °C for 30 min in the dark. The excess DCFH-DA was washed out with PBS prior to metal-complexes exposure at 37 °C for 1 and 3 h. After treatment with compounds the cells were harvested, washed with PBS, lysed by cell dissociation solution (Sigma) and centrifuged to remove cellular debris. The supernatants were transferred in black 96 well plates. The fluorescence generated was measured continuously for 30 min using a Cary Eclipse fluorescence spectrophotometer (Varian, Inc., Palo Alto, CA, USA) (excitation 488 nm, emission 525 nm). Results are expressed as arbitrary absorbance units/mg protein.

#### 2.2.8. Cell cycle

Cell phase distribution was assayed by determining the DNA content of nuclei labeled with propidium iodide (PI) using flow cytometry. Briefly $10^6$ cells were seeded in 25 $cm^3$ flasks. U937 cells in the exponential phase of growth were treated for 24 h with the complexes. Then the cells were collected, washed in PBS, without $Ca^{2+}$ and $Mg^{2+}$ and supplemented with EDTA 0.5 mM, and fixed with 3 mL of 96% ethanol. After fixation, about $1–1.5 \times 10^6$ cells were washed once in PBS and stained in 2 mL of propidium iodide—PI (20 μg/mL in PBS) and 25 μL of RNase-A (1 mg/mL in $H_2O$) at 4 °C overnight. The flow cytometry analysis of the cell cycle was carried out using FACSCalibur (BD, Franklin Lakes, NJ, USA) [34]. Cell cycle phase distribution was calculated as percentages by FlowJo (Tree Star, Inc.)

*2.2.9. Protein determination*

Total protein concentration in cell lysates was assayed by the BCA (bicinchoninic acid) Protein Assay (Thermo Scientific, Rockford, IL, USA), according to the manufacturer's instructions.

*2.2.9.1. P-glycoprotein (Pgp) assay.* Pgp (also known as MDR1 or ABCB1) is an ATP-dependent drug efflux pump, playing an important role in multi-drug resistance. Pgp-Glo™ Assay System (Promega, Madison, WI, USA), a valuable screening tool for determining if a drug interacts with Pgp1, was used to analyze the effects on Pgp ATPase activity. Reagents and reaction mixtures were prepared in accordance with the manufacturer's instructions: 20 μL of assay buffer (Non Treated NT control), of different concentrations of the six compounds (final concentration 5, 10 and 50 μM); of Verapamil (0.5 mM, positive control as Pgp substrate) and of $Na_3VO_4$ (0.25 mM, Pgp inhibitor) dissolved in assay buffer were mixed into the wells of a white opaque 96-well plate (Costar Inc., NY, USA) to Pgp membranes. After a brief incubation at 37 °C for 5 min, the reactions were initiated by the addition of MgATP solution and developed at 37 °C for 40 min. Then the reactions were stopped and luminescence was initiated by adding ATP Detection Reagent to all the wells. Luminescence in all samples was quantified using a Cary Eclipse microtiter plate reader (Varian, Inc., Palo Alto, CA, USA). The decrease in luminescence of NT samples compared to $Na_3VO_4$-treated samples represented the basal Pgp activity and was compared to the difference in average luminescent signals between $Na_3VO_4$-treated samples and samples incubated with the tested compounds, representing Pgp activity in the presence of thiosemicarbazones. The decrease in luminescence of Verapamil-treated samples represented substrate-stimulated Pgp activity.

*2.2.10. Topoisomerase IIα inhibition assay*

The topoisomerase II screening test was performed as previously described [48]: the reaction mixture was prepared by mixing: $H_2O$, topoisomerase reaction buffer, supercoiled DNA substrate, eukaryotic topoisomerase IIα (2 units of activity) and 50 μM solution of compounds (DMSO solution was added to the controls). After incubation at 37 °C for 30 min, the remaining proteins were digested with SDS (10%) and proteinase K. The samples were added with loading dye, then loaded onto a 1% agarose gel and electrophoresed for 5 h at 5 V/cm. The gel was post-stained with TAE solution containing 5 μg/mL ethidium bromide and visualized in a Fluor-S MultiImager (Bio-Rad Laboratories Inc., Hercules, CA, USA).

*2.2.11. Atomic Absorption Spectrometry (AAS)*

Metal concentrations in cellular lysates were determined over a 24 h period of treatment as previously described [48] by means of electrothermal atomic absorption with Zeeman's effect background correction (ETAAS), using a Perkin Elmer Pin AAcle 900Z Atomic Absorption Spectrometer (Waltham, MA, USA). In order to reduce matrix effect certified standards were directly prepared in the supernatant of unexposed cells. The limit of detection (LOD) was 0.05 μg/L.

*2.2.12. Statistical analysis*

Data were expressed as mean + SD of at least three independent experiments. Differences in compounds effects were assessed by means of one-way analysis of variance (ANOVA) followed by Dunnett's or Turkey's post hoc tests. SPSS 17.0 software (SPSS Inc., Chicago, IL, USA) was used and a p value of 0.05 was always considered as significant.

*2.2.13. Partition coefficient calculation*

Log Pow values for the ligands were calculated according to Refs. [35,36].

## 3. Results and discussion

*3.1. Syntheses and spectroscopy*

*trans*-Cinnamaldehyde thiosemicarbazone **1** and cuminaldehyde thiosemicarbazone **2** were prepared according to the synthetic procedure shown in Scheme 1. Their nickel(II) and copper(II) complexes were then prepared according to the synthetic procedure depicted in Scheme 2.

*3.1.1. IR, NMR and UV characterization*

The IR spectrum of Htcin·$H_2O$ **1** is consistent with the expected molecule. The 3100–3500 $cm^{-1}$ region is characterized by a multiplicity of signals assigned to the different NH stretchings, but also to OH stretchings involved in hydrogen bonds, as later confirmed by X-ray diffraction. The iminic C═N stretching, later involved in coordination, is assigned to the 1630 $cm^{-1}$ vibration, even if the region 1630–1600 $cm^{-1}$ is complicated by the presence of the C═C signals involved in conjugation. The 820 $cm^{-1}$ vibrations are attributed to C═S. The IR spectrum of Htcum **2** presents, in the 3100–3500 $cm^{-1}$ region, the vibration assigned to NH stretchings. At 1586 $cm^{-1}$ the iminic C═N stretching is seen and at the 820 $cm^{-1}$ vibration is attributed C═S.

The IR spectrum of [Ni(tcin)$_2$] **3** in the 3100–3500 $cm^{-1}$ region reports few signals with respect to the spectrum of the free ligand, in agreement with the disappearance of one N – H upon deprotonation. The signal at ca 1630 $cm^{-1}$ in the free ligand is shifted at lower wavenumbers as a consequence of the iminic C═N in coordination. A similar behavior is observed for the C═S stretching that is downshifted of ca 40 $cm^{-1}$ foreshadowing a significant bond elongation. As far as [Ni(tcum)$_2$] **4** is concerned, the spectral behavior at high wavenumbers is the same as for **3**; the signal at 1586 $cm^{-1}$ is split into two contributions, at 1603 and 1577 $cm^{-1}$. The absorption at higher wavenumbers can be justified, with the help of the X-ray analysis, to the relevant shortening of the C(═S) – N bond upon coordination and consequent elongation of the C═S bond; for the same reason the C═S stretching is found 25 $cm^{-1}$ downshifted. The spectral behavior of [Cu(tcin)($OH_2$)Cl] **5** is similar to the one of [Ni(tcin)$_2$] **3** in the 3100–3500 $cm^{-1}$ region, due to the deprotonation of the ligand; differences are ascribed to the different patterns of hydrogen bonding. The C═N stretching is found at 1608 $cm^{-1}$, downshifted of ca 20 $cm^{-1}$ with respect to the free ligand and also the C═S stretching is found 12 $cm^{-1}$ lower. The spectral behavior of [Cu(tcum)($OH_2$)Cl] **6** is similar to the one of [Ni(tcum)$_2$] **4** in the 3100–3500 $cm^{-1}$ region, and also for the behavior in the C═C and C═N regions. The C═S vibration is found at 809 $cm^{-1}$ (820 $cm^{-1}$ in the free ligand). The IR spectroscopy of metal complexes is consistent with a coordination via S,N.

The $^1$H NMR spectra of ligands Htcin **1** and Htcum **2** are in agreement with the hypothesized molecules. The hydrazinic N – H is found in both ligands at ca 11.35 ppm, very deshielded as expected, and disappears in both complex spectra with ligand deprotonation. The downfield chemical shift indicates hydrogen bonding with d6-DMSO. The iminic C(H)═N is found at ca 8.16 ppm for both ligands. The two protons of the thiosemicarbazide $NH_2$ are identified as two different resonances at ca 7.91 and 7.61 for Htcin **1** and 8.03 and 7.93 ppm for Htcum **2**. The presence of two resonances means that the free rotation around the C – N bond is blocked because of its partial double bond character [37]. The higher value is assigned to the proton of the hydrogen atom bound to the iminic nitrogen. These observations are in agreement with what already reported [38].

Many differences are seen in the spectra of [Ni(tcin)$_2$] **3**. As already said, the disappearance of the resonance above 11 ppm confirms the deprotonation of the ligand. Terminal $NH_2$ appears as a broad signal, due to the elongation of the C – N bond, at higher fields (ca 7.2 ppm) probably because the hydrogens fall inside the benzene shielding cone [37]. The iminic C(H)═N peak is shifted upfield ($\delta = 0.6$ ppm) compared with the uncomplexed thiosemicarbazone due to the

shielding of the protons via π-back-bonding by the metal center into the azomethine π system. C(H)═C resonances of the unsaturated backbone merged in a unique signal at 6.95 ppm probably due to the extended delocalization following deprotonation and coordination to the metal center. Complex [Ni(tcum)$_2$] **4** behaves in a similar way: the resonance at low field cannot be seen due to deprotonation, terminal $NH_2$ protons merged in a unique signal shifted towards higher fields together with the iminic C(H)═N. All these observation are in agreement with the proposed square planar geometry preserved also in solution.

The UV spectra of the ligands show two absorptions, one of high intensity assignable to n → π* transitions, and one of lower intensity at lower λ attributed to n → σ* transitions. The color of the solutions of the two nickel complexes, brownish, suggests that the complexes are low spin with a square planar geometry [39] in the tested solvents (DMSO, $CH_3OH$, DMSO/$H_2O$ mixtures) as already seen by NMR, and confirming that the coordination geometry is preserved in the different solvents. The spectral behavior of the two nickel complexes is similar, even though the absorptions are more noticeable in [Ni(tcin)$_2$] **3**, whereas in [Ni(tcum)$_2$] **4** the lower frequency bands appear as shoulders of the main absorption peaks. The DMSO solution of the copper(II) complexes is dark green and brownish; their UV spectra show two bands for [Cu(tcin)($H_2O$)Cl] **5**, whereas for [Cu(tcum)($H_2O$)Cl] **6** three bands are present, in agreement with Ref. [39], and their square planar geometry is probably tetrahedrally distorted.

*3.1.2. Circular dichroism*

To establish in more detail if the binding of the complexes brings about any significant conformational change of the DNA double helix, CD spectra of CT-DNA were recorded at increasing complex/CT-DNA ratios. The observed CD spectrum of natural calf thymus DNA consists of a positive band at 280 nm (UV: λ max, 260 nm) due to base stacking and a negative band at 250 nm due to helicity, which is characteristic of DNA in its right-handed B form. It is known that at wavelengths above 230 nm the CD spectrum of B form consists of a longwave positive and a shortwave negative band of nearly equal magnitude with an intersection point at the absorption maximum [40]. This interpretation, generally reported in the literature, is not correct from a spectroscopic point of view. In fact, coupling of the transition moments of chromophores leads to a bisignate CD curve centered at the absorption maximum (260 nm in this case). The couplet with positive first, at longer wavelengths, and negative second Cotton effects, respectively, is defined as a positive couplet [41] and corresponds, in this case, to the right helix of the B-form of DNA. The effect of the compounds on the conformation of the secondary structure of DNA was studied by keeping constant the concentration of CT-DNA at $5 \cdot 10^{-5}$ M [NP] and by varying the concentration of the metal complex in a buffer solution of 10 mM of PBS (pH = 7.4) 137 mM NaCl, 2.7 mM KCl (r = [complex]/[DNA] = 0, 0.1, 0.2, 0.4, 0.6). The spectrum of the CT-DNA and those in the presence of the compounds were monitored in the range 220 to 320 nm. In the CD

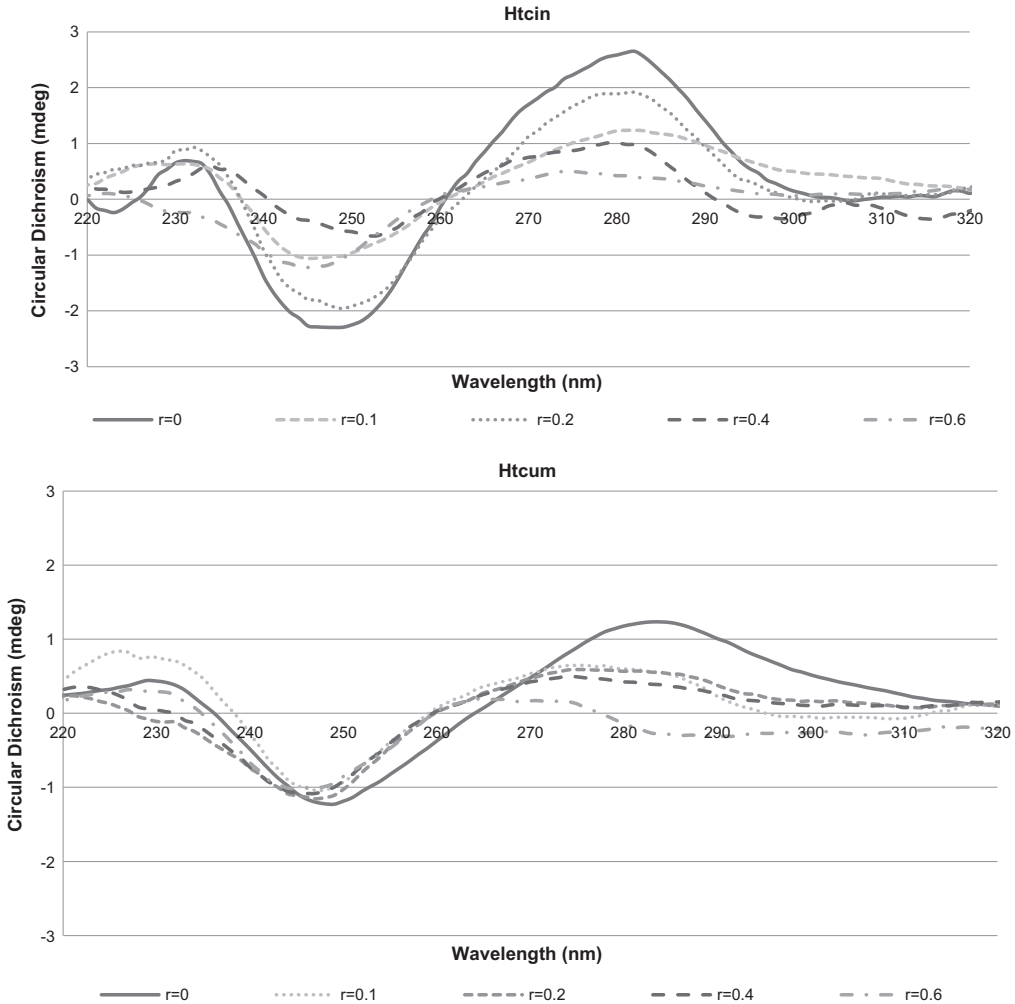


**Fig. 1.** CD spectra of CT-DNA treated with ligand Htcin **1** (above) and with ligand Htcum **2** (below) with r = [ligand] / [DNA] = 0; 0.1; 0.2; 0.4; 0.6.

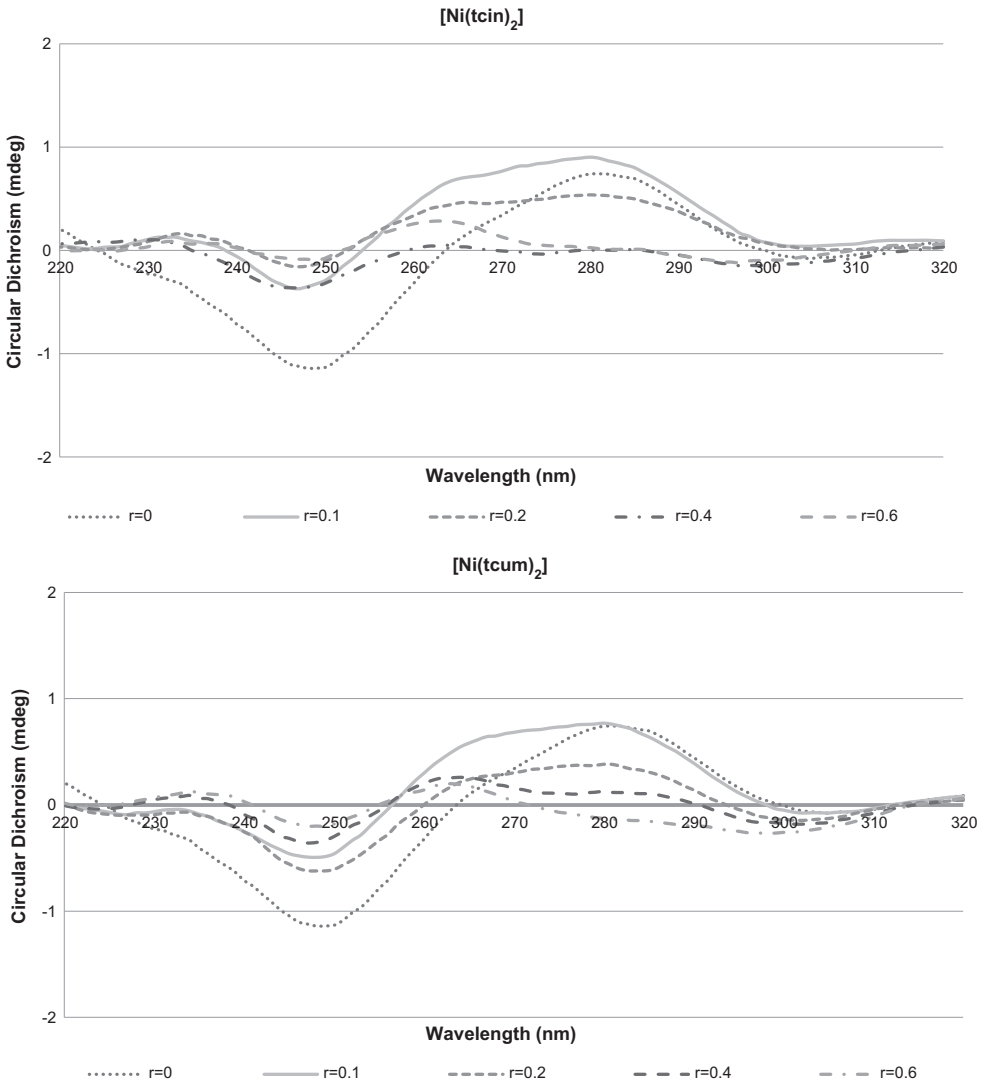


**Fig. 2.** CD spectra of CT-DNA treated with nickel(II) complexes: $[Ni(tcin)_2]$ (above) and with complex $[Ni(tcum)_2]$ (below) with r = [complex] / [DNA] = 0; 0.1; 0.2; 0.4; 0.6.

spectrum of ligand Htcin **1** (Fig. 1) the decrease of intensity of the negative band is not directly correlated to the increase of the compound quantity. On the other hand, the intensity decrease of the positive band is more related to the variation of its concentration. This behavior suggests the existence of possible weak interactions between the nucleic acid and the molecule.

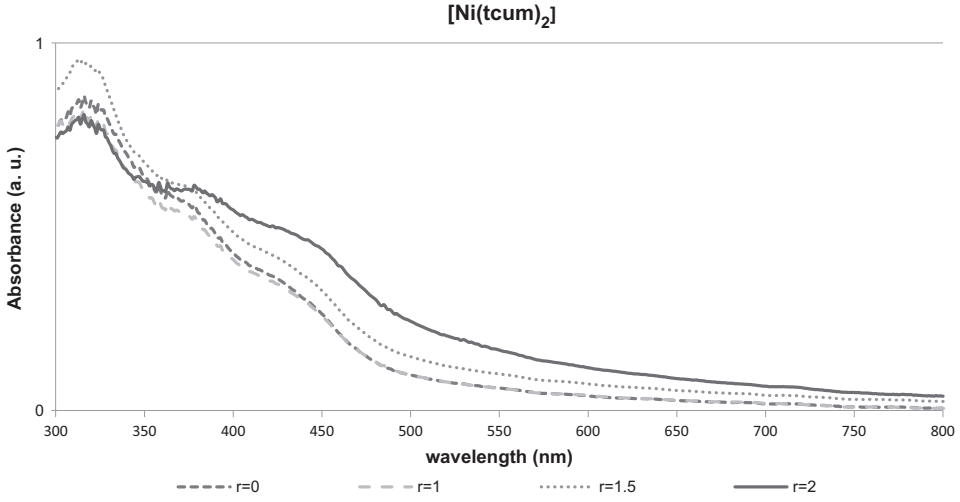


**Fig. 3.** Absorption titration curves for $[Ni(tcum)_2]$ **4** at different [DNA]/[complex] ratios. The [complex] is constant at $4.0 \cdot 10^{-5}$ M.

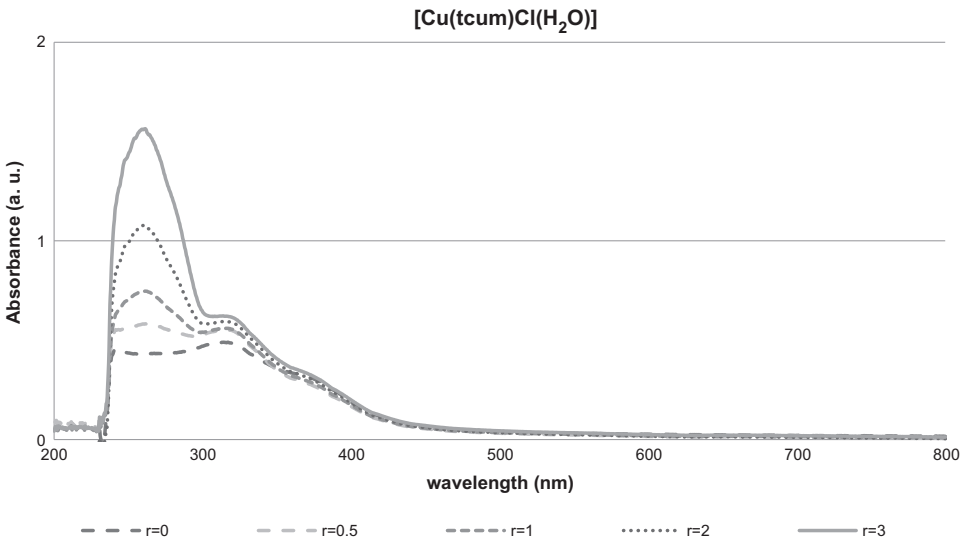


**Fig. 4.** Absorption titration curves for [Cu(tcum)Cl($H_2O$)] **6** at different [DNA]/[complex] ratios. The [complex] parameter is kept constant at $1.0 \cdot 10^{-3}$ M.

As far as ligand Htcum **2** is concerned, we observe a negligible change in the negative band, while following an increase of the ratio [complex]/[DNA] there is a significant decrease in the positive signal until almost disappearance (Fig. 1). In the literature [42] this trend is associated with a change in conformation of native DNA from B to C.

As shown in Fig. 2 for the nickel complexes, the CD spectrum of DNA exhibits a monotonous decrease of the band at ca. 250 nm together with a light red shift for both nickel(II) complexes. The effect is more pronounced for [Ni(tcin)$_2$] **3** than for [Ni(tcum)$_2$] **4**. A major change can be observed for the positive band at ca. 280 nm. If simple groove binding and electrostatic interactions with small molecules show less of a perturbation or no perturbation whatsoever on the base stacking and helicity bands [43], in our case both metal complexes show a deep interaction with DNA.

The dichroic spectral behaviors are consistent with a possible B (native state) to C conformational change [40] where the positive band is practically absent. The absence of isodichroic points also suggests that more than one DNA-complex species could be present at the same moment. Moreover, at low complex-to-DNA molar ratio, the presence of a shoulder centered at around 260 nm with a positive Cotton effect could also suggest the presence of the A form of DNA, even though less prominent than the former. This latter fact could also explain the reason why the negative band is modified, while in the C form shape, location and magnitude are more similar to those for the B form. This deviation is more evident for [Ni(tcin)$_2$] **3** than for [Ni(tcum)$_2$] **4** and this trend could be in agreement with an enhanced flexibility of the cinnamaldehyde derivative with respect to cuminaldehyde one, and this trend also agrees with what is already observed for ligand **1**. Moreover, the CD spectral behavior of [Ni(tcum)$_2$] could also be consistent with a drift giving rise to a condensed Ψ-DNA form [44–46]. In fact, the stereochemical peculiarities of the binding to DNA imply a transition of the macromolecule conformation. The conformational transitions facilitate the adduct formation. It has been already observed that the C conformation of DNA can gradually transform into a chiral Ψ phase [46]. In GC-DNA, Ni(II) binds strongly and specifically to the N7 atom of guanine in the major groove and induces a conformational change of the backbone from B- to Z-DNA, where the N7 atom of guanine is more accessible. This conformational change takes place at submillimolar concentrations of Ni(II) cations, as confirmed by the CD and OD measurements [47]. In the present work we did not observe any transition from B to Z conformation, as found for the interaction of CT-DNA (GC content = 42%) with different metal complexes [48]. It is also known that Ni(II) induces a complete condensation of GC rich DNA [47]. From these observations we can assume that the interaction

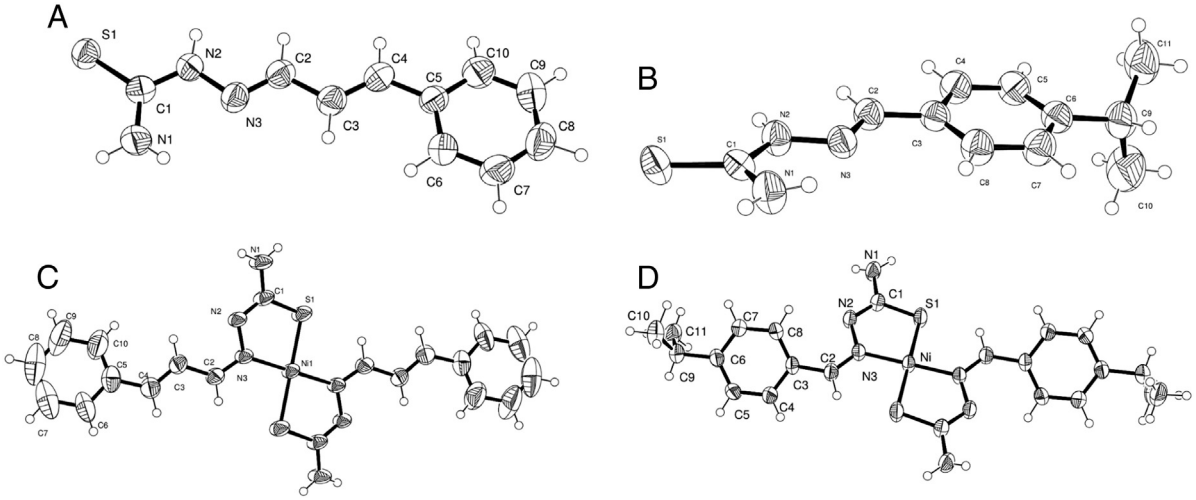


**Fig. 5.** Ortep view of Htcin **1** (A), Htcum **2** (B), [Ni(tcin)$_2$] **3** (C) and [Ni(tcum)$_2$] **4** (D). Ellipsoids are at 50% probability level.

**Table 2**
Selected bond lengths (Å) and angles (°) for compounds **1**–**4**.

| | Ligand **1** | Ligand **2** | Complex **3** | Complex **4** |
|---|---|---|---|---|
| S(1) – C(1) | 1.706(3) | 1.675(2) | 1.725(4) | 1.718(2) |
| N(1) – C(1) | 1.312(4) | 1.294(2) | 1.331(5) | 1.349(3) |
| N(2) – C(1) | 1.325(4) | 1.333(2) | 1.305(5) | 1.308(3) |
| N(2) – N(3) | 1.383(3) | 1.362(2) | 1.403(4) | 1.401(2) |
| N(3) – C(2) | 1.269(4) | 1.262(2) | 1.294(5) | 1.293(3) |
| C(2) – C(3) | 1.445(4) | 1.442(2) | 1.434(5) | 1.464(3) |
| C(3) – C(4) | 1.321(5) | | 1.323(5) | |
| C(4) – C(5) | 1.464(4) | | 1.454(6) | |
| Ni1 – S1 | | | 2.170(1) | 2.166(1) |
| Ni1 – N3 | | | 1.892(3) | 1.930(2) |
| S1 – Ni1 – N3 | | | 86.0(1) | 86.2(1) |

towards the nucleic acid cannot be ascribed to the Ni(II) ion action. Moreover, from the spectroscopic pattern, an intercalative mechanism can be excluded. Therefore, what we observe is that the tested complex induces conformational modifications of DNA that may determine also the functional ones. Generally speaking, CD results are indicative of deep conformational changes of the DNA double helix following the interaction of the DNA macromolecule with the metal complex.

The CD spectral behavior of Cu(II) complexes is similar to those previously described. As already observed for the free ligand Htcin **1** and partially also for its Ni(II) complex [Ni(tcin)$_2$] **3**, the decrease of intensity of the negative band is not directly correlated to the increase of the compound concentration. On the other hand, the intensity decrease of the positive band is more sensitive to the variation of the complex concentration. This behavior suggests that, also in this case, an interaction between the nucleic acid and the molecule cannot be excluded, but in any case it is a weak interaction. Also in the case of the complex [Cu(tcum)(H$_2$O)Cl] **6**, there is an analogy in the behavior of the free ligand and the Ni(II) complex. We observe a negligible change in the negative band, while with the increase of the ratio [complex]/[DNA] there is a significant decrease in the positive signal until almost extinction. As already noted, this trend, in the literature [42], is associated with a change in conformation of native DNA from B to C.

Summing up, from CD experiments, as far as Htcin **1** and its Ni(II) and Cu(II) complexes are concerned, DNA seems to be a negligible target; only [Ni(tcin)$_2$] **3** seems to give a somewhat appreciable

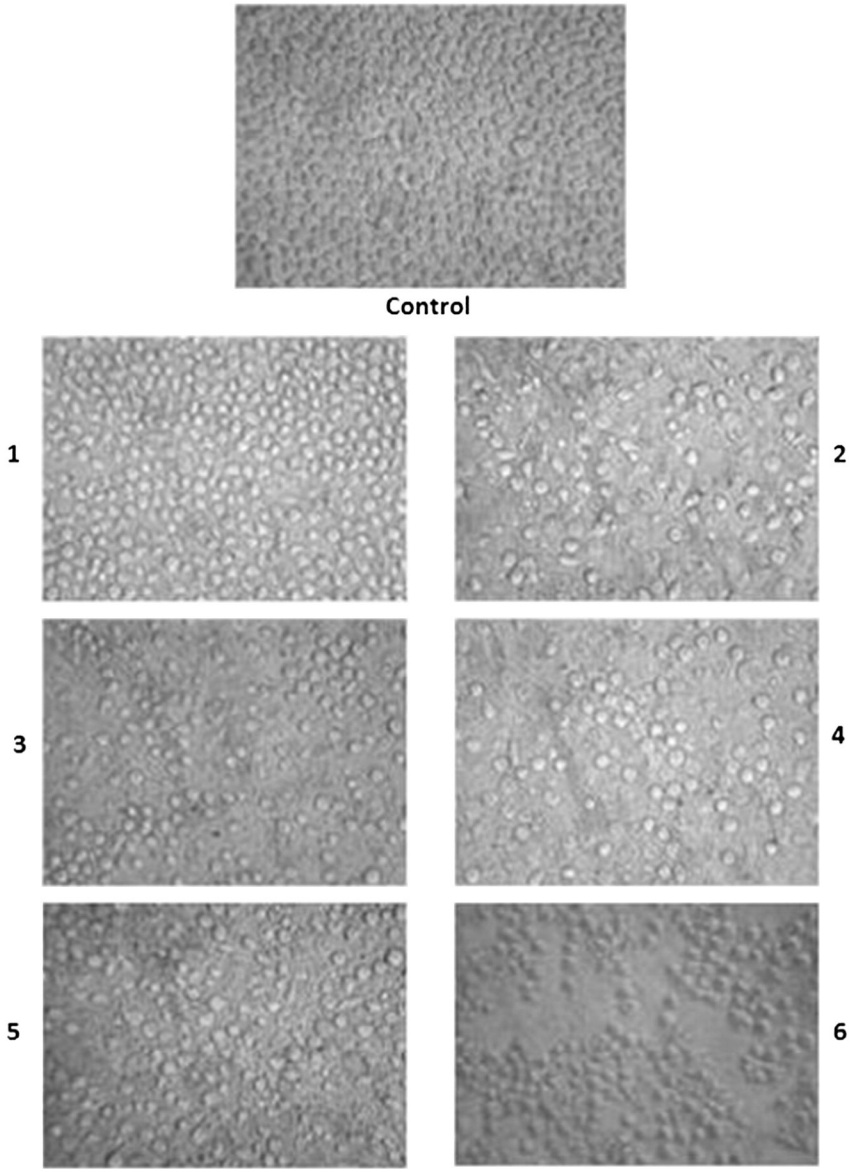


**Fig. 6.** Cytotoxic effects after 24 h treatments. U937 cells were cultured in medium containing $IC_{50}$ concentrations of ligands or complexes and observed under optical microscopy (200×).

interference. As far as Htcum **2** and its Ni(II) and Cu(II) complexes are concerned, on the other hand, all compounds seem to induce severe modification in DNA conformation, promoting a structure change from B to C as far as the complex-to-DNA molar ratio increases. Nickel complex [Ni(tcum)$_2$] **4** is the compound that seems to act more profoundly on the nucleic acid.

*3.1.3. UV titrations*

Binding constants for the interaction of the studied compounds with nucleic acid were determined by means of UV–vis titrations as described in the literature [49]. These studies were carried out on both ligands and on their Ni(II) and Cu(II) complexes. The intrinsic binding constant Kb for the interactions with CT-DNA of the compounds under

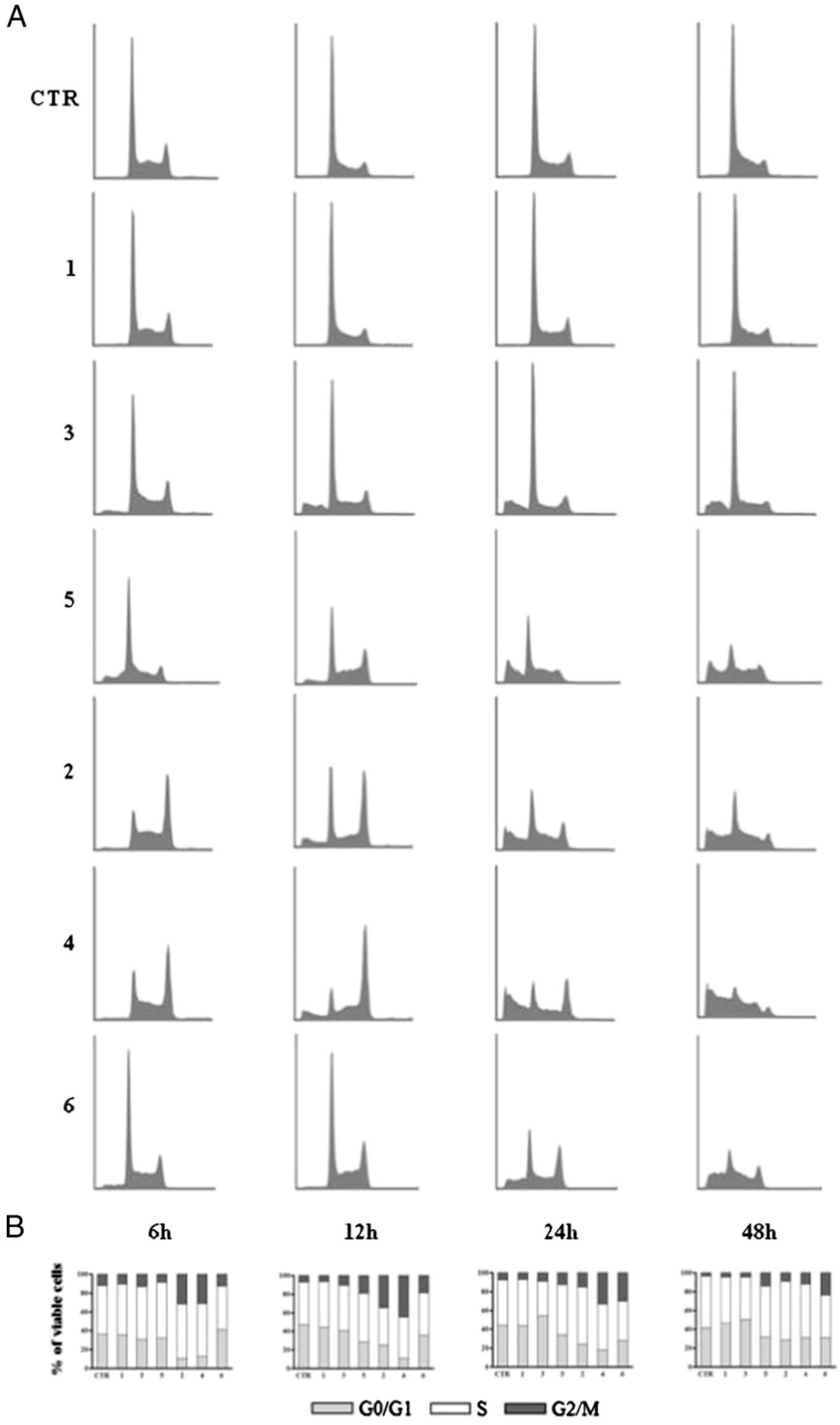


**Fig. 7.** Effects of Htcin **1**, [Ni(tcin)$_2$] **3**, [Cu(tcin)Cl(H$_2$O)] **5** and Htcum **2**, [Ni(tcum)$_2$] **4**, [Cu(tcum)Cl(H$_2$O)] **6** on cell cycle distribution of U937 cells. Exponentially growing cells were treated with IC$_{50}$ concentrations of the ligands and of their metal complexes for 6, 12, 24 and 48 h. A: Biparametric forward/side scatter, monoparametric DNA cell cycle analysis with percentages of U937 cells. Four distinct phases can be recognized in the proliferating cell population, corresponding to different peaks: the $G_1$-, S- (DNA synthesis phase), $G_2$- and M-phases (mitosis). B: Histograms represent the distribution of U937 cells, treated with compounds **1**, **3**, **5**, **2**, **4** and **6** respectively, in the different phase of the cycle. ▭ G0/G1 phase; ▭ S phase; G2/M phase. Sub G0/G1 cell population (corresponding to apoptotic cells or cellular debris) was not included in the analysis.

study was calculated by absorption spectra titration data using the following equation: $1 / \Delta\varepsilon_{ap} = 1 / (\Delta\varepsilon K_b D) + 1 / \Delta\varepsilon$ where $\Delta\varepsilon_{ap} = |\varepsilon_A - \varepsilon_f|$, $\Delta\varepsilon = |\varepsilon_B - \varepsilon_f|$, D = [DNA], and $\varepsilon_A$, $\varepsilon_B$, and $\varepsilon_f$ are the apparent, bound, and free extinction coefficients of the compound, respectively. The constant $K_b$ is given by the ratio of the slope to intercept when it is reported in plot [DNA]/($\varepsilon_A - \varepsilon_f$) versus [DNA] and is expressed in $M^{-1}$. Fixed amounts of the ligands and of the complexes were dissolved in DMSO, because their high solubility in this solvent allowed us to prepare concentrated solutions and therefore to utilize reduced volumes in titrations. It was also verified that the DMSO percentage added to the DNA solution did not interfere with the nucleic acid; in fact, the 260 nm absorption band is not subject to modifications in intensity and position. Calculated amounts of stock solutions were taken to final concentration values of 10 mM of PBS (pH = 7.4) 137 mM NaCl, 2.7 mM KCl, and increasing amounts of DNA over a range of ratios (r = [DNA] / [compound]) from 0 to 3 keeping the compound concentration constant at $1.0 \cdot 10^{-3}$ M for Htcin **1**, $9.8 \cdot 10^{-4}$ M for Htcum **2**, $4.5 \cdot 10^{-5}$ M for [Ni(tcin)$_2$] **3**, $4.0 \cdot 10^{-5}$ M for [Ni(tcum)$_2$] **4**, $1.0 \cdot 10^{-3}$ M for [Cu(tcin)($H_2O$)Cl] **5** and $1.0 \cdot 10^{-3}$ M for [Cu(tcum)($H_2O$)Cl] **6**. The compounds were titrated at room temperature after 1 h incubation. The changes in absorbance of an intraligand (IL) band upon each addition of DNA were monitored at the maximum wavelengths (nm) 329 for Htcin **1**, 313 nm for Htcum **2**, 328 for [Ni(tcin)$_2$] **3**, 329 [Ni(tcum)$_2$] **4**, 436 for [Cu(tcin)($H_2O$)Cl] **5** and 314 for [Cu(tcum)($H_2O$)Cl] **6**. From the titration spectra of the ligands it was observed that they give no relevant interaction with DNA, inducing to think that the ligands do not give rise to stable or strong association with the nucleic acid; we therefore focused our attention on the analysis of the complexes. It is interesting to note that the spectral behavior of [Ni(tcin)$_2$] **3** and [Ni(tcum)$_2$] **4** treated with increasing amount of DNA, monitored at 329 nm and 436 nm respectively, shows the absorption increasing as r increases (Fig. 3). In the case of [Ni(tcum)$_2$] **4**, at other wavelengths we observe an opposite behavior (Fig. 3). In any case the differences in absorbance between the free complexes and the complexes completely bound to DNA are not enough to determine a significant $k_b$ value. As sensed by the CD experiment, probably there is a multiple way of action of the Ni(II) complex able to perturb the DNA structure, more evident for [Ni(tcum)$_2$] **4** than for [Ni(tcin)$_2$] **3**.

The binding constant $k_b$ obtained for [Cu(tcin)Cl($H_2O$)] **5** and for [Cu(tcum)Cl($H_2O$)] **6** are 26 $M^{-1}$ and 30 $M^{-1}$ respectively. The values we found show that the interaction between the nucleic acid and the copper complexes is weak even though stronger if compared with the action exerted by the free ligand. Probably the metal center has a role in driving the molecule nearer to the target where it can interact through hydrogen bonds or Coulomb forces. The spectral behavior of [Cu(tcum)Cl($H_2O$)] **6** treated with increasing amount of DNA reported in Fig. 4 shows in any case that an interaction is present.

The relatively lower $k_b$ value found for [Cu(tcin)($H_2O$)Cl] **5** is attributable to the role of the spacer between the aromatic moiety and the metal center. Our results show that someway there is a concentration dependence on the action of the metal complexes on DNA. Hyperchromism shows that an external mode of binding cannot be excluded; different modes of bindings were already presumed from CD studies. It is of relevance to observe that for both CD and UV–vis studies, the role of the cinnamaldehyde chain on the thiosemicarbazone induces less relevant changes in its behavior towards the nucleic acid.

### 3.2. Crystal structures

#### 3.2.1. Htcin·$H_2O$ (*1*) and Htcum (*2*)

The molecular structures of **1** and **2** are represented in Fig. 5, A and B respectively. For ligand **1**, comparing the corresponding bond distance values with those reported in Ref. [23], where the same compound was studied at room temperature, it was observed, as expected, to have shorter values. Ligand **1** displays a wide planarity induced by an extended system of conjugated double bonds and also stabilized by the intramolecular hydrogen bond N1…N3 2.619(5) Å. The dihedral angle between the thiosemicarbazide chain and the aromatic ring is 10.7°. The ligand shows an E conformation relative to the C1 – N2 bond. A molecule of crystallization water is involved in hydrogen bonds [N2…O1W 2.824(4) Å, N2-H…O1W 174(3)°, O1W…S1 (x − 1, +y, +z) 3.301(3) Å, O1W-H…S1 177(4)°, O1W…S1(x − 1/2, −y + 1/2 + 2, −z + 2) 3.289(4) Å, O1W-H13…S1 165(4)°] so determining dimeric layers parallel to the (001) plane. Also in compound **2** the sulfur atom and the hydrazine nitrogen N3 are in *trans* position with respect to the C1 – N2 bond and the molecular conformation is determined by the presence of the strong intramolecular hydrogen bond between the imine and the amine nitrogens N1…N3 2.616(2) Å. The dihedral angle between the thiosemicarbazidic chain and the cuminaldehyde ring is 9.84°. The isopropyl group is bent with respect the aromatic ring forming a dihedral angle of 88°. The packing is characterized by a three-dimensional network of hydrogen bonds [N2…S1(−x, −y + 2, −z) 3.35(2) Å, N2-H…S1 159(2)°, N1…S1(−x, y − 1/2, −z − 1/2) 3.363(2) Å, N1 – H…S1 178(2)°].

#### 3.2.2. Ni(tcin)$_2$·2$C_2H_5OH$ (*3*) and Ni(tcum)$_2$ (*4*)

Both complexes **3** and **4** consist of the neutral molecules [Ni(tcin)$_2$] and [Ni(tcum)$_2$] with the metal placed on a symmetry center. The

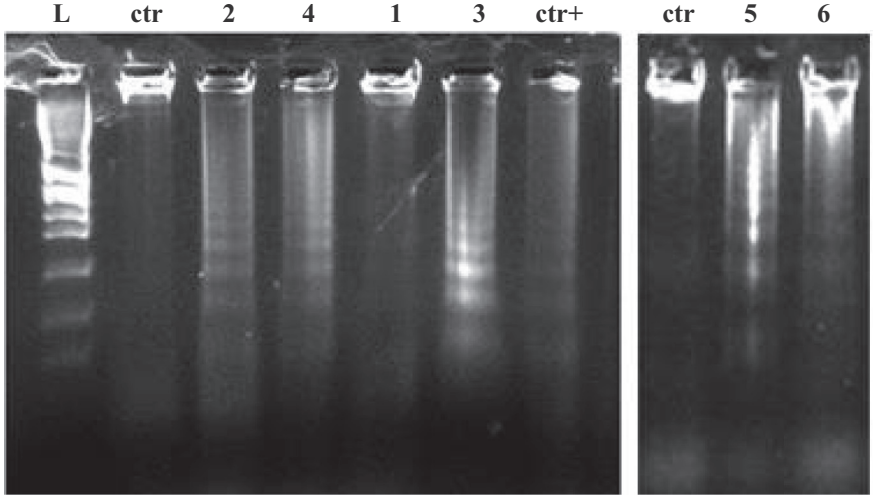


**Fig. 8.** Agarose gel electrophoresis of cellular DNA stained by ethidium bromide. Lane L = Ladder; CTR = untreated control cells; $CTR^+$ = positive control (U937 cells treated with 2 μg/mL anisomycin for 3 h).

coordination results in a square distorted configuration which involves the sulfur atom and the imine atom N3 of the two deprotonated ligands (Fig. 5, C and D).

The ligands **1** and **2**, upon coordination to the metal, change their *E* conformations into *Z* and behave as bidentate through the S1 and the iminic N3. The metal to donor distances are only slightly different: the Ni1 – S1 bonds are 2.170(1) Å and 2.166(1) Å and the Ni1 – N3 bonds 1.892(3) Å and 1.930(2) Å for **3** and **4** respectively and agree well with those generally found in square complexes of nickel(II) thiosemicarbazones [23,50]. The corresponding S1 – Ni1 – N3 angles are also quite similar: 86.0(1)° in the first and 86.2(1)° in the second. Another feature that these two compounds have in common is a major delocalization of charge with respect to the free ligands (Table 2) due to deprotonation of the hydrazinic N2 atom, nevertheless the angle between the thiosemicarbazide chain and the aromatic ring is 27.9(1)° and 29.3(1)°, bigger than in the free ligands (10.7° and 9.8°). In complex $[Ni(tcum)_2]$ **4** the isopropyl group is bent with respect the aromatic ring forming a dihedral angle of 89.7(2)°. Only in compound **3** two centrosymmetrical disordered ethanol molecules of crystallization are present. These molecules govern the packing by hydrogen bonds involving the oxygen and the aminic nitrogen [N1…O1(−x, −y + 2, −z) 2.932(6) Å, N1-H…O1 173.1(3)°, N1…O1(x + 1, y, z) 2.967(4) Å, N1-H…O1 162.0(2)°]. The ethanol molecule also acts as a bridge between two centrosymmetrical complexes forming the layers. The aromatic rings protrude from these sheets. In complex **4** only a weak hydrogen bond N1…N2(x − 1/2, −y + 1/2, z) 3.114(3) Å, N1-H…N2 159(2)° is present.

### 3.3. Biological tests

Differences in U937 cell morphology were observed between Htcum, $[Ni(tcin)_2]$, $[Ni(tcum)_2]$, $[Cu(tcin)(H_2O)Cl]$, and $[Cu(tcum)(H_2O)Cl]$ treated and control cells by light microscopy. The most conspicuous change observed included nuclear condensation and formation of apoptotic bodies (Fig. 6). These changes, which are characteristic of cell apoptotic death, were visible after 6 h treatment, and were absent in the control and in Htcin exposed cells. The morphological change became more remarkable with time progression and drug concentration. Images shown here were photographed after 24 h treatment (other time points are not shown). The effects of ligands and complexes on cell growth and viability assessed by the commonly used MTS assay at different intervals (6, 12, 24, 48 h) of exposure were confirmed by Trypan blue exclusion: Htcum, $[Ni(tcum)_2]$, $[Ni(tcin)_2]$, $[Cu(tcin)(H_2O)Cl]$ and $[Cu(tcum)(H_2O)Cl]$ treatments significantly inhibited the growth and affected viability of U937 cells in both concentration- and time-dependent manners whereas no cytotoxic effect was detected also at the highest concentrations of Htcin. At 24 h the $IC_{50}$ value was

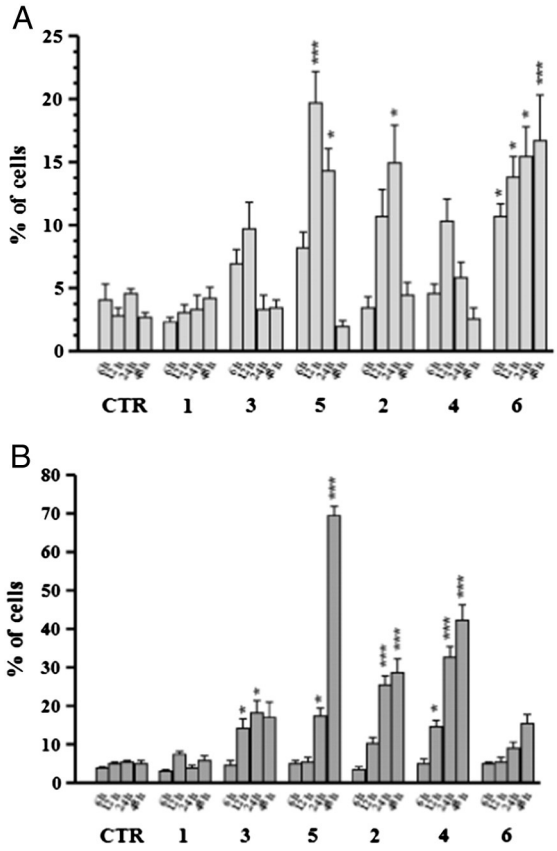


**Fig. 9.** Early (A) and late (B) apoptosis induced by ligands and complexes. Annexin V-FITC(+)/PI(−) stained U937 cells have been considered early apoptotic cells and the Annexin V-FITC(+)/PI(+) cell population necrotic or advanced apoptotic. Results represent the mean (±SD) of three separate experiments carried out in duplicate (vs control * = p < 0.05, ** = p < 0.01, *** = p < 0.001) at 6, 12, 24 and 48 h respectively.

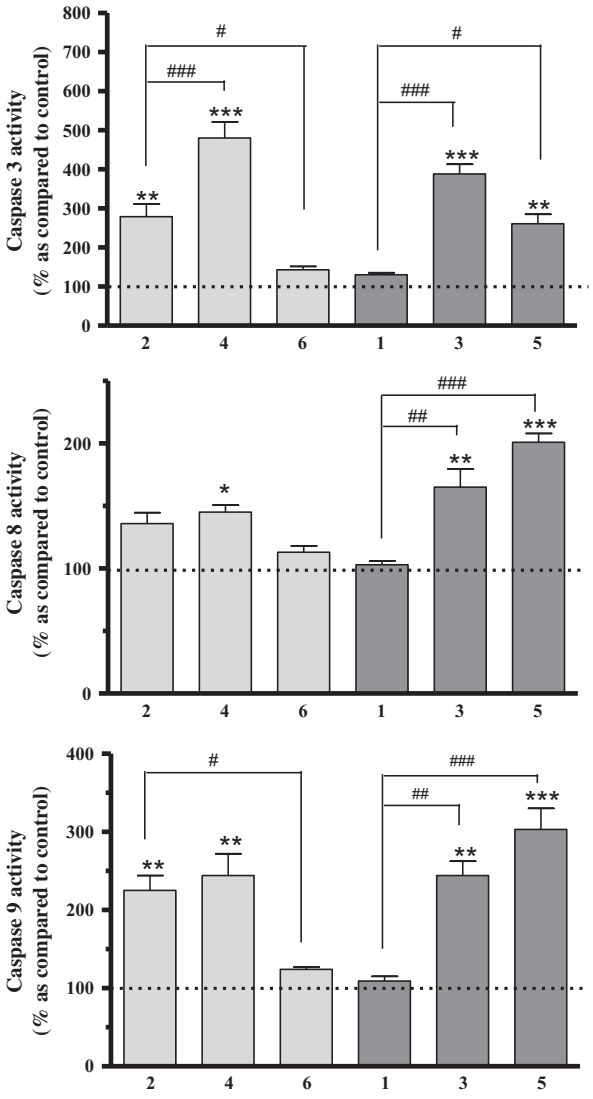


**Fig. 10.** Caspase activities were measured after 12 h (caspase-8 and -9) and after 24 h (caspase-3). Percentage vs control = (sample value / control value) × 100. Results represent the mean (±SD) of three separate experiments carried out in duplicate (vs control * = p < 0.05, ** = p < 0.01, *** = p < 0.001 — vs ligand # = p < 0.05, ## = p < 0.01, ### = p < 0.001).

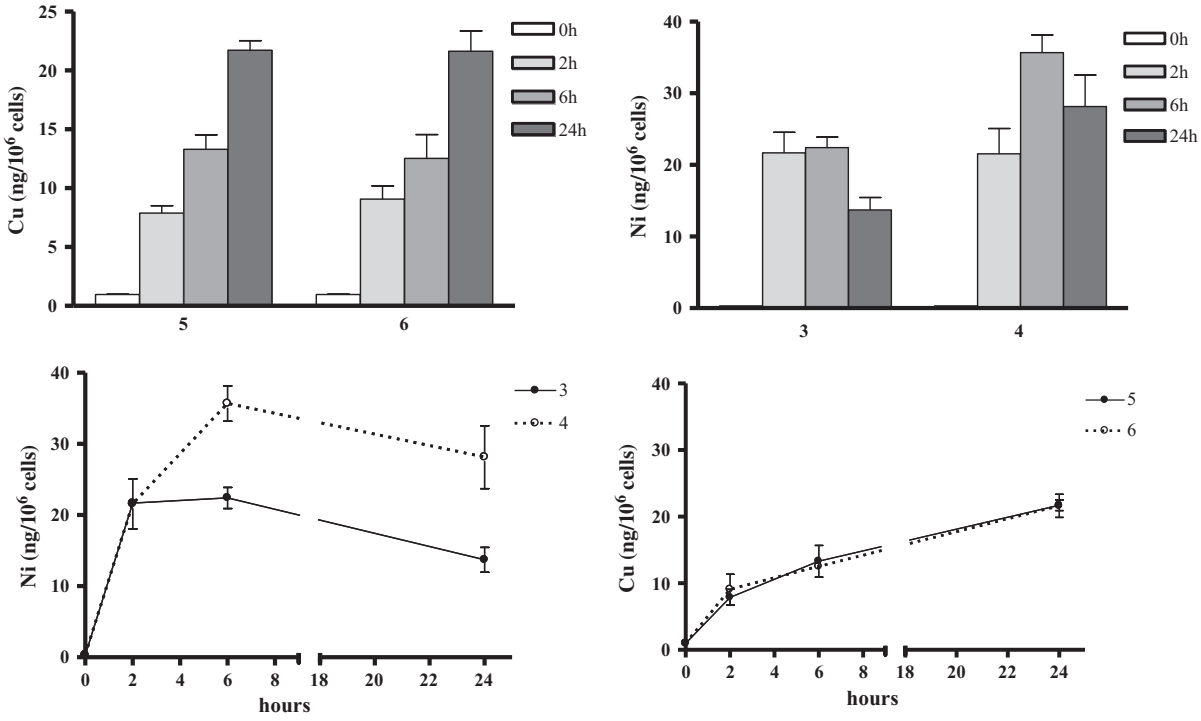


**Fig. 11.** Evaluation uptake in U937 cells treated with the same concentration (2 μM) of the metal complexes. Intracellular Ni and Cu were measured over a 24 h period. Results are shown as means ± SD.

3.2 (±0.28) μM for **2**, 5.9 (±0.05) μM for **4**, 7.8 (±0.74) μM for **6**, 8.1 (±0.55) μM for **3** and 3.3 (±.61) μM for **5**, respectively. The effects of exposure to the compounds on the viability of U937 were compared with those determined on human fibroblasts (non-cancer cells): ligands and complexes were much less active on this primary line, as evidenced by the $IC_{50}$ values ($IC_{50}$ > 100 μM for **1**, **2**, **3**, and **4**; $IC_{50}$ = 66.95 ± 2.64 μM for **5** and 52.81 ± 2.57 μM for **6**). To test whether ligands or complexes could affect the cell cycle, U937 cells treated with $IC_{50}$ doses for 24 h were subjected to flow cytometric analysis after DNA staining. As shown in Fig. 7, exposure to Htcum, [Ni(tcum)$_2$] and [Cu(tcum)Cl($H_2O$)] resulted in an increase in the $G_2$/M phase, that was accompanied by a decrease in the $G_0/G_1$ phase, and in a progressive accumulation of cells in sub-$G_0/G_1$ phase. For example, the percentage of G2/M phase increased by 5- and 6.4-fold on 12 h treatment of cells with Htcum and [Ni(tcum)$_2$] compared with control: these compounds caused $G_2$/M phase cell cycle arrest. Htcin did not modify the cell cycle: in the representative histograms depicting cell cycle distribution in U937 cultures exposed to [Ni(tcin)$_2$] a sub G0/G1 peak was observed, corresponding to apoptotic cells, and a slight increased percentage of G0/G1 resting cells. Treatment with [Cu(tcin)($H_2O$)Cl] caused more relevant modifications of the cell cycle. Cell cycle arrest has been reported to correlate with induction of apoptosis. Based on our cell cycle analysis data, further studies were carried out to demonstrate the effect of the studied compounds on apoptosis induction, through DNA fragmentation analysis, to confirm the underlying mechanism behind their inhibitory activity on the cell cycle. Treatment with $IC_{50}$ doses of Htcum(**2**), [Ni(tcum)$_2$](**4**), [Cu(tcum)($H_2O$)Cl](**6**), induced DNA fragmentation after 24 h. In the series Htcin (**1**), [Ni(tcin)$_2$](**3**) and [Cu(tcin)($H_2O$)Cl](**5**), the complexes gave the DNA ladders with multiple bands that characterize apoptosis, while for ligand (**1**) no DNA bands were detected (Fig. 8). Additional evidence for the occurrence of apoptosis was obtained by double staining of the cultures with PI and Annexin V-FITC. Annexin V binds with high affinity to phosphatidylserine, which is translocated from the inner to the outer membrane leaflet early in the apoptotic process. As shown in Fig. 9 untreated and Htcin treated cells were Annexin V-FITC and PI negative, indicating that they were viable and not undergoing apoptosis. On the other hand, after 12 h of incubation with compounds **2**, **3**, **4**, **5**, and **6**, a significant increase of Annexin V-positive, PI-negative cells, was observed indicating that they were in the early stages of apoptosis. At 24 and 48 h the decrease of early apoptotic cells and the corresponding strong increase of the double positive stained cells revealed the progression towards a late apoptotic stage or

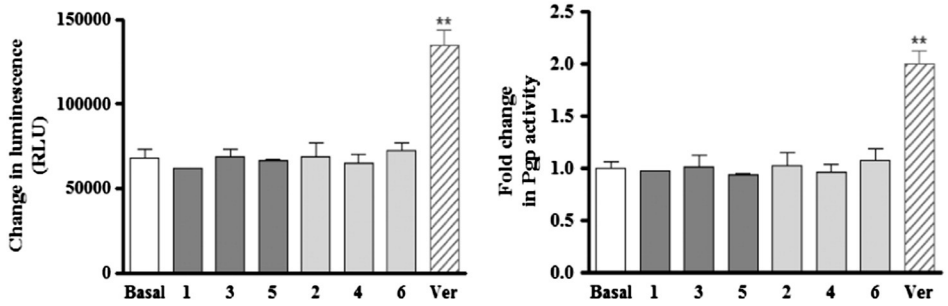


**Fig. 12.** Effects of the six compounds on Pgp ATPase activity. Results are expressed as means ± SD of differences between the relative luminescence units (RLU) measured or results (means ± SD) are compared to the basal activity: ΔRLU of test compound and of Verapamil (Ver) / ΔRLUbasal. Significantly different from basal activity: ** = $p < 0.01$.

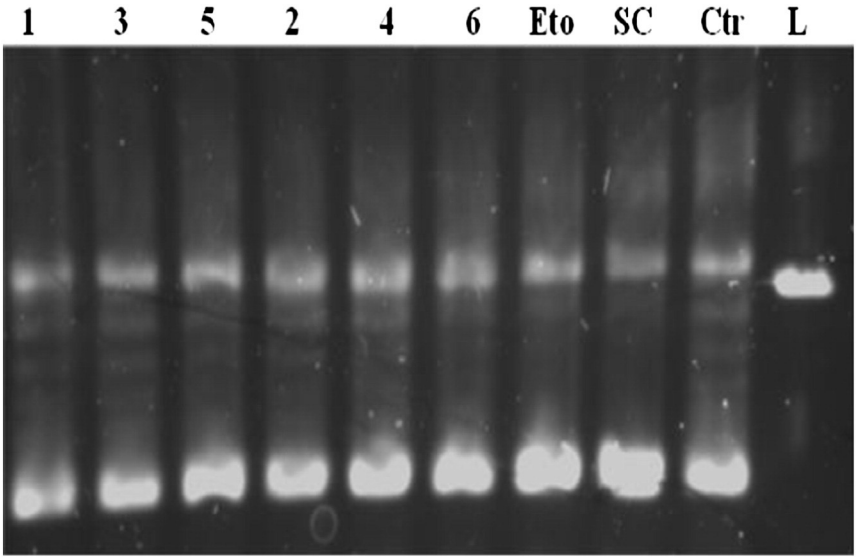


**Fig. 13.** Agarose gel-based topoisomerase-IIa inhibition assay. Lanes: L linear DNA, CTR topoisomerase-IIa +, SC supercoiled DNA, ETO Etoposide; lanes 1–6 denote the reaction of Topo-IIα with supercoiled DNA in presence of 10 μM of compounds **1**, **3**, **5**, **2**, **4**, and **6**.

necrosis. This progression was later during exposure to [Cu(tcum)($H_2O$)Cl]: at 48 h the early apoptotic population was still increasing (Fig. 9). The molecular mechanism underlying the potent pro-apoptotic effects on U937 cells was further studied, monitoring the intracellular levels of caspases. As showed in Fig. 10 Htcum, [Ni(tcum)$_2$] and [Ni(tcin)$_2$] and [Cu(tcin)($H_2O$)Cl] significantly activated caspase-9 and caspase-3. Caspase-8 activity was significantly induced by [Ni(tcin)$_2$] and [Cu(tcin)($H_2O$)Cl] whereas exposure to Htcum, [Ni(tcum)$_2$] resulted in slight increases of caspase-8 activity, significant only for the complex. The slight activation of caspases in the early stages of exposure to [Cu(tcum)($H_2O$)Cl] was in agreement with the later apoptosis progression observed. These results indicated that activation of caspase cascade might play a crucial role in apoptosis induction and that different mechanisms underlie the cytotoxic and apoptotic effects of the different compounds.

Intracellular Ni and Cu concentrations were determined over a 24 h period of treatment in order to verify if compounds could be pumped out of the cells. It was observed that there is no decrease in cell lysates of complexed metals, (Fig. 11) in agreement with the result that the compounds neither activate nor inhibit Pgp protein activity (Fig. 12).

The topoisomerase IIa inhibition test was carried out for all the compounds. As it can be seen in Fig. 13, the capacity of copper complexes is apparent in compound **6** in particular, to inhibit the enzyme to the same extent shown by etoposide, a compound usually taken as a reference.

In order to measure the role of compounds in inducing intracellular oxidation, an oxidation sensitive fluorescent dye called DCFH-DA was used as this leads to an increase in fluorescent intensity upon generation of intracellular ROS. In U937 cells no such an increase was observed at any of the studied doses of ligands or complexes (data not shown).

In order to verify if the difference in the biological activity among the two ligands could be related to an enhanced ability of Htcum **2** to enter the cell with respect to Htcin **1**, the partition octanol/water coefficient was calculated. The logP values found were 2.09 ± 0.47 for Htcin **1** and 2.93 ± 0.37 for Htcum **2**, suggesting that the simple diffusion through the cell membrane cannot be the answer to the enhanced biological activity of **2** with respect to **1**.

## 4. Conclusions

Thiosemicarbazones derived from cinnamaldehyde and cuminaldehyde were synthesized and characterized together with their Ni(II) and Cu(II) metal complexes. The compounds were tested in vitro for their antileukemic activity on U937 human cell line. The results were multifaceted: ligand Htcin **1** was unable to exert any effect even at high concentrations while ligand Htcum **2** inhibited cell proliferation with an $IC_{50}$ value of 3.2 μM. All the metal complexes have very low $IC_{50}$ values ([Ni(tcin)$_2$] 8.1 μM; [Ni(tcum)$_2$] 5.9 μM; [Cu(tcin)($H_2O$)Cl] 3.3 μM; [Cu(tcum)($H_2O$)Cl] 5.9 μM), especially taken into account the $IC_{50}$ exerted on the same cell line by the most famous metal based drug cisplatin (6.6 μM). The compounds tested on human fibroblasts showed no activity or activity at very high $IC_{50}$ values. It is noteworthy that in the case of cinnamaldehyde derivatives, upon coordination to metal ions, the bioactivity dramatically increases confirming that complexation can be an interesting strategy for dose reduction. Htcum and all the nickel and copper complexes induce apoptosis. A lower percentage of late apoptotic cells was observed during [Ni(tcin)$_2$] treatment with respect to [Ni(tcum)$_2$] or Htcum which revealed the progression towards a late apoptotic stage or necrosis. This progression was later instead during exposure to [Cu(tcum)($H_2O$)Cl] where at 48 h the early apoptotic population was still increasing. Htcum and [Ni(tcum)$_2$] and [Cu(tcum)($H_2O$)Cl] caused $G_2$/M phase cell cycle arrest suggesting a possible action on topoisomerase II, while for [Ni(tcin)$_2$] a sub $G_0/G_1$ peak was observed, corresponding to apoptotic cells, and a slight increased percentage of $G_0/G_1$ resting cells. It was confirmed that the copper complexes and [Cu(tcum)($H_2O$)Cl] in particular are able to inhibit topoisomerase IIa activity. If Htcum, [Ni(tcum)$_2$], [Ni(tcin)$_2$] and [Cu(tcin)($H_2O$)Cl] significantly activated caspase-9 and caspase-3, caspase-8 activity was significantly induced only by [Ni(tcin)$_2$] and [Cu(tcin)($H_2O$)Cl]. From these data it seems that the intrinsic pathway is preferred, even if the activation of caspase-8 by [Ni(tcin)$_2$] and [Cu(tcin)($H_2O$)Cl] does not allow us to exclude an extrinsic pathway. The slight activation of caspases in the early stages of exposure to [Cu(tcum)($H_2O$)Cl] is in agreement with the later apoptosis progression observed. From the tests carried out directly on DNA it results that the nucleic acid is not a main target for the molecules under study, even if, especially for the Ni(II) complexes, it comes out that they can perturb its conformation. On the other hand, the tests also show that whenever DNA should be reached by the metal complexes, the action exerted on it is not due to the metal ion alone. It was verified that the compounds are not pumped out of the cells. Cuminaldehyde derivatives and cinnamaldehyde metal complexes are therefore good candidate to be explored for their in vivo antileukemic activity.

*Abbreviations*

| | |
|---|---|
| AAS | Atomic Absorption Spectroscopy |
| BCA | Bicinchoninic Acid |
| CT DNA | Calf Thymus DNA |
| DCFH-DA | 2,7-Dichlorofluorescein Diacetate |
| DCFH | 2′,7′-Dichlorofluorescein |
| ETAAS | Electrothermal Atomic Absorption Spectrometry |
| FBS | Fetal Bovine Serum |
| Htcin | *trans*-Cinnamaldehyde Thiosemicarbazone |
| Htcum | Cuminaldehyde Thiosemicarbazone |
| LOD | Limit of Detection |
| PBS | Phosphate Buffered Saline |
| Pgp | Permeability Glycoprotein |
| ROS | Reactive Oxygen Species |

## Acknowledgments

The authors wish to thank the CIM (Centro Interdipartimentale Misure) "Giuseppe Casnati" of the University of Parma for NMR facilities and Prof. Marisa Belicchi-Ferrari for her constant presence during the preparation of the paper.

## Appendix A. Supplementary data

Supplementary data to this article can be found online at http://dx.doi.org/10.1016/j.jinorgbio.2014.07.014. These data include MOL files and InChiKeys of the most important compounds described in this article.

## References

[1] G.M. Cragg, D.J. Newman, Biochim. Biophys. Acta 1830 (2013) 3670–3695.
[2] B.M. Kwon, S.H. Lee, S.U. Choi, S.H. Park, C.O. Lee, Y.K. Cho, N.D. Sung, S.H. Bok, Arch. Pharm. Res. 21 (1998) 147–152.
[3] C.M. Cabello, W.B. Bair, S.D. Lamore, S. Ley, A.S. Bause, S. Azimian, G.T. Wondrak, Free Radic. Biol. Med. 46 (2009) 220–231.
[4] T. Nitoda, M.D. Fan, I. Kubo, Phytother. Res. 22 (2008) 809–813.
[5] N.S. Moorthy, N.M. Cerqueira, M.J. Ramos, P.A. Fernandes, Recent Pat. Anticancer Drug Discov. 8 (2013) 168–182.
[6] H. Beraldo, D. Gambino, Mini-Rev. Med. Chem. 4 (2004) 31–39.
[7] B.M. Paterson, P.S. Donnelly, Chem. Soc. Rev. 40 (2011) 3005–3018.
[8] G. Pelosi, Open Crystallogr. J. 3 (2010) 16–28.
[9] Y. Yu, E. Gutierrez, Z. Kovacevic, F. Saletta, P. Obeidy, Y.S. Rahmanto, D.R. Richardson, Curr. Med. Chem. 19 (2012) 2689–2702.
[10] F. Bisceglie, M. Baldini, M. Belicchi Ferrari, E. Buluggiu, M. Careri, G. Pelosi, S. Pinelli, P. Tarasconi, Eur. J. Med. Chem. 42 (2007) 627–634.
[11] M.B. Ferrari, F. Bisceglie, G. Pelosi, M. Sassi, P. Tarasconi, M. Cornia, S. Capacchi, R. Albertini, S. Pinelli, J. Inorg. Biochem. 90 (2002) 113–126.
[12] D. Kovala-Demertzi, A. Papageorgiou, L. Papathanasis, A. Alexandratos, P. Dalezis, J.R. Miller, M.A. Demertzis, Eur. J. Med. Chem. 44 (2009) 1296–1302.
[13] G.L. Parrilha, J.G. da Silva, L.F. Gouveia, A.K. Gasparoto, R.P. Dias, W.R. Rocha, D.A. Santos, N.L. Speziali, H. Beraldo, Eur. J. Med. Chem. 46 (2011) 1473–1482.
[14] M. Belicchi-Ferrari, F. Bisceglie, A. Buschini, S. Franzoni, G. Pelosi, S. Pinelli, P. Tarasconi, M. Tavone, J. Inorg. Biochem. 104 (2010) 199–206.
[15] F. Bisceglie, S. Pinelli, R. Alinovi, P. Tarasconi, A. Buschini, F. Mussi, A. Mutti, G. Pelosi, J. Inorg. Biochem. 116 (2012) 195–203.
[16] A. Buschini, S. Pinelli, C. Pellacani, F. Giordani, M.B. Ferrari, F. Bisceglie, M. Giannetto, G. Pelosi, P. Tarasconi, J. Inorg. Biochem. 103 (2009) 666–677.
[17] P. Tarasconi, S. Capacchi, G. Pelosi, M. Cornia, R. Albertini, A. Bonati, P.P. Dall'Aglio, P. Lunghi, S. Pinelli, Bioorg. Med. Chem. 8 (2000) 157–162.
[18] Q.X. Chen, K.K. Song, Q. Wang, H. Huang, J. Enzym. Inhib. Med. Chem. 18 (2003) 491–496.
[19] Y.J. Zhu, K.K. Song, Z.C. Li, Z.Z. Pan, Y.J. Guo, J.J. Zhou, Q. Wang, B. Liu, Q.X. Chen, J. Agric. Food Chem. 57 (2009) 5518–5523.
[20] P.M. Krishna, K.H. Reddy, Inorg. Chim. Acta 362 (2009) 4185–4190.
[21] P.M. Krishna, K.H. Reddy, J.P. Pandey, D. Siddavattam, Transit. Met. Chem. 33 (2008) 661–668.
[22] A.G. Quiroga, J.M. Perez, I. Lopez-Solera, J.R. Masaguer, A. Luque, P. Roman, A. Edwards, C. Alonso, C. Navarro-Ranninger, J. Med. Chem. 41 (1998) 1399–1408.
[23] Y.M. Chumakov, N.M. Samus, G. Bocelli, K.Y. Suponitskii, V.I. Tsapkov, A.P. Gulya, Russ. J. Coord. Chem. 32 (2006) 14–20.
[24] P.P.T. Sah, T.C. Daniels, Recl. Trav. Chim. Pays-Bas 69 (1950) 1545–1556.
[25] G. Sheldrick, SADABS. Program for Empirical Absorption Correction of Area Detector, University of Göttingen, Göttingen, 1996.
[26] A. Altomare, M.C. Burla, M. Camalli, G.L. Cascarano, C. Giacovazzo, A. Guagliardi, A.G.G. Moliterni, G. Polidori, R. Spagna, J. Appl. Crystallogr. 32 (1999) 115–119.
[27] G. Sheldrick, SHELXL 97. A Program for Structure Refinement, University of Göttingen, Göttingen, 1997.
[28] L.J. Farrugia, J. Appl. Crystallogr. 32 (1999) 837–838.
[29] M. Nardelli, J. Appl. Crystallogr. 28 (1995) 659.
[30] A.L. Spek, PLATON, A Multipurpose Crystallographic Tool, University of Utrecht, Utrecht, 1998.
[31] C.F. Macrae, I.J. Bruno, J.A. Chisholm, P.R. Edgington, P. McCabe, E. Pidcock, L. Rodriguez-Monge, R. Taylor, J. van de Streek, P.A. Wood, J. Appl. Crystallogr. 41 (2008) 466–470.
[32] M.E. Reichmann, S.A. Rice, C.A. Thomas, P. Doty, J. Am. Chem. Soc. 76 (1954) 3047–3053.
[33] S. Tagliaferri, A. Caglieri, M. Goldoni, S. Pinelli, R. Alinnovi, D. Poli, C. Pellacani, G. Giordano, A. Mutti, L.G. Costa, Toxicol. in Vitro 24 (2010) 116–122.
[34] E. Erba, D. Bergamaschi, L. Bassano, G. Damia, S. Ronzoni, G.T. Faircloth, M. D'Incalci, Eur. J. Cancer 37 (2001) 97–105.
[35] VCCLAB, Virtual Computational Chemistry Laboratory, http://www.vcclab.org 2005.
[36] I.V. Tetko, J. Gasteiger, R. Todeschini, A. Mauri, D. Livingstone, P. Ertl, V.A. Palyulin, E.V. Radchenko, N.S. Zefirov, A.S. Makarenko, V.Y. Tanchuk, V.V. Prokopenko, J. Comput. Aided Mol. Des. 19 (2005) 453–463.
[37] M.B. Ferrari, S. Capacchi, G. Reffo, G. Pelosi, P. Tarasconi, R. Albertini, S. Pinelli, P. Lunghi, J. Inorg. Biochem. 81 (2000) 89–97.
[38] A. Diaz, I. Garcia, R. Cao, H. Beraldo, M.M. Salberg, D.X. West, L. Gonzalez, E. Ochoa, Polyhedron 16 (1997) 3549–3555.
[39] M.J.M. Campbell, Coord. Chem. Rev. 15 (1975) 279–319.
[40] V.I. Ivanov, L.E. Minchenkova, A.K. Schyolkina, A.I. Poletayev, Biopolymers 12 (1973) 89–110.
[41] R.V. Person, K. Monde, H.U. Humpf, N. Berova, K. Nakanishi, Chirality 7 (1995) 128–135.
[42] C.A. Sprecher, W.A. Baase, W.C. Johnson Jr., Biopolymers 18 (1979) 1009–1019.
[43] B. Norden, F. Tjerneld, Biopolymers 21 (1982) 1713–1734.
[44] J. Kypr, I. Kejnovska, D. Renciuk, M. Vorlickova, Nucleic Acids Res. 37 (2009) 1713–1725.
[45] A. Silvestri, G. Barone, G. Ruisi, D. Anselmo, S. Riela, V.T. Liveri, J. Inorg. Biochem. 101 (2007) 841–848.
[46] N.J. Zuidam, Y. Barenholz, A. Minsky, FEBS Lett. 457 (1999) 419–422.
[47] J.C. Sitko, E.M. Mateescu, H.G. Hansma, Biophys. J. 84 (2003) 419–431.
[48] S. Mahadevan, M. Palaniandavar, Chem. Commun. (1996) 2547–2548.
[49] A. Wolfe, G.H. Shimer Jr., T. Meehan, Biochemistry 26 (1987) 6392–6396.
[50] F.H. Allen, O. Kennard, Chem. Des. Autom. News (1993) 31–37.